

Inclusion of $K\Lambda$ electroproduction data in a coupled channel analysis

M. Mai,^{1,2,*} J. Hergenrather,² M. Döring,^{2,3} T. Mart,⁴ Ulf-G. Meißner,^{1,5,6} D. Rönchen,⁵ and R. Workman²
(Jülich-Bonn-Washington Collaboration)

¹*Helmholtz-Institut für Strahlen- und Kernphysik (Theorie) and Bethe Center for Theoretical Physics, Universität Bonn, 53115 Bonn, Germany*

²*Institute for Nuclear Studies and Department of Physics, The George Washington University, Washington, DC 20052, USA*

³*Thomas Jefferson National Accelerator Facility, Newport News, VA 23606, USA*

⁴*Departemen Fisika, FMIPA, Universitas Indonesia, Depok 16424, Indonesia*

⁵*Institute for Advanced Simulation and Jülich Center for Hadron Physics, Forschungszentrum Jülich, 52425 Jülich, Germany*

⁶*Tbilisi State University, 0186 Tbilisi, Georgia*

Exclusive electroproduction reactions provide an access to the structure of excited baryons. To extract electroproduction multipoles encoding this information, the Jülich-Bonn-Washington (JBW) analysis framework is extended to the analysis of differential cross sections in $K\Lambda$ electroproduction. This update enlarges the scope of previous coupled-channel analyses of pions and eta mesons, with photoproduction reactions as boundary condition in all analyzed electroproduction reactions. Polarization observables are predicted and compared to recent CLAS data. The comparison shows the relevance of these data to pin down baryon properties.

I. INTRODUCTION

Electromagnetic probes of strongly interacting matter provide independent access to emergent phenomena of Quantum Chromodynamics (QCD) like resonances. Photoproduction reactions have been used to determine the spectrum and properties of excited baryons [1, 2] as analyzed by different groups [3–10]. These analyses allow for a comparison to theory like lattice QCD [11–21] or quark models [22–28]. See Ref. [29] for a recent review. Notably, first calculations of meson-baryon scattering amplitudes in lattice QCD have appeared recently, some of them containing the $\Delta(1232)3/2^+$ resonance [30–34]. Complementary to photoproduction reactions, radiative decays of excited baryons, such as measured by CLAS [35], can reveal information about their nature, see, e.g., Refs. [36–38].

In addition, the momentum transfer of the probe can be tuned once the photon is allowed to become virtual, testing strong interactions at different scales. Indeed, electroproduction reactions are a prime tool to study the structure of excited baryons [39, 40]. One cannot directly test the response of a resonance to a virtual photon, but determine transition form factors in the electroexcitation of the resonance from the nucleon. One can map out the transverse charge density by using electromagnetic form factors [41]. The Q^2 -dependent multipoles can also be used to test chiral perturbative calculations [42–49] and unitary extensions [50–52], chiral resonance calculations [53, 54], and quark models [55–62]. Notably, a gauge invariant chiral unitary framework for kaon electroproduction was developed in Ref. [63] and extended later [64, 65]. Transition form factors also serve as

point of comparison for dynamical quark calculations referred to as Dyson-Schwinger approaches [66–71]. In this context, remarkable agreement of the lower-lying baryon spectrum with predictions has been achieved [69, 71], showing little evidence for a “missing resonance” problem at lower energies. See Refs. [72–76] for reviews. Methods to study the Q^2 -dependence of resonance couplings in lattice QCD were proposed in Ref. [77]. A pioneering lattice calculation was carried out recently in the meson sector [78].

Transition form factors have been defined in different ways [72], but the only reaction-independent definition is given in terms of Q^2 -dependent couplings at the resonance pole, to be determined by an analytic continuation of electroproduction multipoles [79].

The multipoles themselves are determined by analyzing the exclusive electroproduction of one or more mesons. The advantage of simultaneously analyzing different final states in a coupled-channel approach lies in the factorization of the amplitude at the pole, i.e., the fact that the resonance transition form factor is the same for any final state.

Another reason to perform global analyses of electroproduction reactions is the need to analyze as many data simultaneously as possible. The data situation in electroproduction reactions tends to be more challenging than in photoproduction. On one hand, this is due to the presence of another kinematic variable in addition to the energy W , namely the virtuality of the photon $Q^2 = -q^2$, where q is the transferred four-momentum of the photon. Even though the number of data points is larger in electro- than in photoproduction, the data are still sparser due to this additional variable. On the other hand, there are longitudinal multipoles to be determined from data, in addition to the electric and magnetic ones that parameterize the photoproduction amplitudes. The related question of how many measurements

* mai@hiskp.uni-bonn.de

are necessary to determine a truncated partial-wave expansion of the electroproduction amplitude is discussed in Refs. [80, 81].

All this motivates the inclusion of $K\Lambda$ electroproduction reported in this paper. This coupled-channel extension is based on previous analyses within the Jülich-Bonn-Washington (JBW) framework of pion [82] and eta-meson [83] electroproduction. Representing the first coupled-channel electroproduction analysis, data at the photon point ($Q^2 = 0$) are also included as a boundary condition from previous analysis of pion [9], eta [84], and $K\Lambda$ [85] photoproduction. The model was recently extended to $K\Sigma$ photoproduction [86] and pion-induced ω productions [87], but the analysis presented here is based on the JüBo2017 solution that includes πN , ηN , and $K\Lambda$ photoproduction. In addition, the coupled-channel amplitude was also used to simultaneously analyze the pion-induced production of the aforementioned meson-baryon states [88, 89], providing additional constraints on the strong final-state interactions in both photo- and electroproduction. The comparisons of data and fit solutions of pion- and real-photon-induced reactions (JüBo) have been collected on a website [90]. The JBW electroproduction solutions are collected on another interactive website [91].

The single-channel analysis of single-meson electroproduction data has a long history; one of the first approaches is MAID for pion photo- and electroproduction [5, 92], later complemented by a chiral-MAID approach at low energies [93]. There is also the eta-MAID2001 analysis on eta electroproduction [94]. See Ref. [95] for a review. The CLAS collaboration extracted helicity amplitudes for several resonances from their experiment [96], including the unusual zero in the $A_{1/2}$ Roper form factor [97, 98]; see also Refs. [99, 100] for other CLAS analyses. The ANL-Osaka group analyzed electroproduction data in the context of neutrino-induced reactions [101]. Questions on efficient parametrizations of electroproduction amplitudes and transition form factors are discussed in Refs. [102–104]. The two-pion electroproduction reaction has also been measured at CLAS and analyzed with the JM reaction model [105–108], see also Ref. [109]. Notably, much higher Q^2 values for resonance transition form factors become accessible in ongoing CLAS12 experiments [73].

Most relevant for the present analysis of $K\Lambda$ electroproduction is KAON-MAID [3, 110], an analysis using an effective Lagrangian approach [111], and the more recent analyses using a Regge-plus-resonance (RPP) amplitude [112, 113]. See Ref. [114] for an overview of kaon electroproduction reactions and Refs. [115–121] for related analyses and theoretical developments by JPAC and others.

In the present analysis we fit mostly cross section data for $\gamma^* p \rightarrow K\Lambda$ from CLAS. Notably, the data base was recently enlarged through the addition of beam-recoil transfer polarization data [122]. In the presented update of the JBW approach, we predict the latter data but do

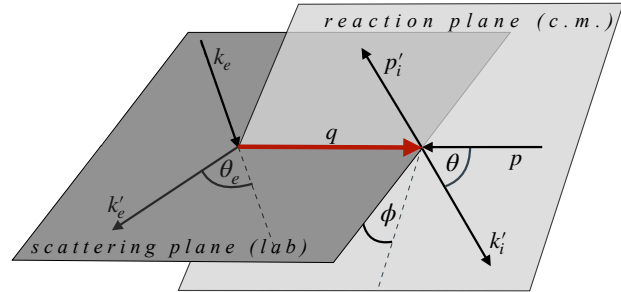


FIG. 1. Kinematics of an electroproduction experiment with the final meson-baryon state i . The scattering plane is defined by the respective in/outgoing electron momenta k_e/k'_e with the electron scattering angle θ_e . The reaction plane is spanned by the virtual photon and the outgoing meson, scattered by an angle θ . The momenta q and p correspond to the virtual photon and target nucleon while k'_i and p'_i correspond to the outgoing meson and baryon, respectively.

not fit them. This allows for a check of how much they will constrain the multipole extraction in future analyses, for which $K\Sigma$ electroproduction data should also be included. As $K\Lambda$ electroproduction requires an extension to higher energies, we enlarge the range of analyzed electroproduction data accordingly from $W = 1.6$ GeV to $W = 1.8$ GeV, compared to the previous study [83]. Also, the range in Q^2 was extended up to $Q^2 = 8$ GeV² for all analyzed final states, and we also include F-waves now, owing to the higher energy range. The extraction of resonance transition form factors is scheduled once the analysis stage is complete.

This study is organized as follows. Section II outlines formal aspects of the JBW approach to pseudo-scalar meson electroproduction. Furthermore, we define the parametrization of the Q^2 dependence connected to the photon point at $Q^2 = 0$, where the underlying JüBo model describes photon- and meson-induced reactions. Section III describes the data and fit procedures with different data weighting. Section IV compares our fits to data and puts the analysis in context.

II. FORMALISM

We summarize the formalism following closely Refs. [82, 83] in a more general form. The multichannel meson electroproduction process under consideration is

$$\gamma^*(\mathbf{q}) + p(\mathbf{p}) \rightarrow M(\mathbf{k}'_i) + B(\mathbf{p}'_i), \quad (2.1)$$

where bold symbols denote three-momenta throughout the manuscript. The meson and baryon in the final state, with the index i , are denoted by M and B , respectively. As shown in Fig. 1, the process occurs in two

steps, with a virtual photon $\gamma^*(\mathbf{q})$ being produced via $e_{\text{in}}(\mathbf{k}_e) \rightarrow e_{\text{out}}(\mathbf{k}'_e) + \gamma^*(\mathbf{q})$, which then scatters off the proton to a final meson-baryon state. The momentum transfer $Q^2 = -\omega^2 + \mathbf{q}^2$, where ω is the photon energy, is non-negative for spacelike processes, and acts as an independent kinematical variable in addition to the total energy in the center-of-mass (c.m.) frame, W . In this frame, the magnitude of the three-momentum of the photon ($q = |\mathbf{q}|$) and produced meson ($k'_i = |\mathbf{k}'_i|$) read

$$q = \frac{\sqrt{\lambda(W^2, m_p^2, -Q^2)}}{2W}, \quad k'_i = \frac{\sqrt{\lambda(W^2, m_i^2, M_i^2)}}{2W}, \quad (2.2)$$

where $\lambda(x, y, z) = x^2 + y^2 + z^2 - 2xy - 2yz - 2zx$ denotes the usual Källén triangle function. Meson and baryon masses are denoted by M and m , respectively. With two incoming and three outgoing particles there are $(3 + 2) \times 3 - 10 = 5$ independent kinematic variables. The canonical choice for the remaining three (in addition to W and Q^2) variables is illustrated in Fig. 1. The quantity ϵ is defined through

$$\epsilon = \frac{1}{1 + 2(q_L^2/Q^2) \tan^2 \theta_e/2}, \quad (2.3)$$

and contains the electron scattering angle θ_e and q_L denotes the photon three-momentum in the laboratory frame. The angle of the reaction plane to the scattering plane is given by ϕ , and θ is the c.m. meson scattering angle in the latter plane. The experimental data discussed in Sec. III, symbolized as O , are represented with respect to these five variables, i.e., $O(Q^2, W, \phi, \theta, \epsilon)$.

As discussed in the previous paper [82], based on the seminal works [123–126], the process of a photon-induced production of a meson off a nucleon is encoded in the transition amplitude. In the one-photon approximation, and considering the continuity equation for the current, the latter can be expressed in terms of three independent multipoles for a fixed quantum number ℓ_{\pm} of the final meson-baryon state. We chose those to be electric, magnetic and longitudinal multipoles $E_{\ell_{\pm}}^{\mu}(W, Q^2)$, $M_{\ell_{\pm}}^{\mu}(W, Q^2)$ and $L_{\ell_{\pm}}^{\mu}(W, Q^2)$ with the latter related to the often-used Coulomb multipole as $\omega C_{\ell_{\pm}}(W, Q^2) = qL_{\ell_{\pm}}(W, Q^2)$. Each of these multipoles carries a discrete index corresponding to the total angular momentum $J = \ell \pm 1/2$ and final-state index μ , e.g., $E_{0+}^{\eta p}$.

We construct the electroproduction multipoles on the basis of the dynamical coupled-channel Jülich-Bonn (JüBo) approach [9, 89] that provides the boundary condition at $Q^2 = 0$, incorporating the experimental information from real-photon and pion-induced reactions. In this approach, two-body unitarity and analyticity are respected and the baryon resonance spectrum is determined in terms of poles in the complex energy plane on the second Riemann sheet [127, 128]. In particular, we use the JüBo2017 solution that includes πN , ηN , and $K\Lambda$ photoproduction [85].

Extending the ansatz of the JüBo approach, we begin by introducing a generic function (\mathcal{M}) for each electromagnetic multipole ($\mathcal{M}_{\mu\gamma^*} \in \{E^{\mu}, M^{\mu}, L^{\mu}\}$) as

$$\begin{aligned} \bar{\mathcal{M}}_{\mu\gamma^*}(k, W, Q^2) &= V_{\mu\gamma^*}(k, W, Q^2) \\ &+ \sum_{\kappa} \int_0^{\infty} dp p^2 T_{\mu\kappa}(k, p, W) G_{\kappa}(p, W) V_{\kappa\gamma^*}(p, W, Q^2), \end{aligned} \quad (2.4)$$

where μ is a channel index and the summation extends over intermediate meson-baryon channels $\kappa \in \{\pi N, \eta N, K\Lambda, K\Sigma, \pi\Delta, \rho N\}$. Note that the σN channel is not part of this list. The σN channel is part of the final-state interaction, but neither the hadronic resonance vertex functions nor the photon is directly coupled to it. However, once photo- or electroproduction data of the $\pi\pi N$ final state are analyzed, such couplings will become relevant and will be included. Note that we have suppressed isospin and the angular momentum index ℓ_{\pm} in Eq. (2.4).

The electroproduction kernel $V_{\mu\gamma^*}$ in Eq. (2.4) is parameterized as

$$\begin{aligned} V_{\mu\gamma^*}(p, W, Q^2) &= \alpha_{\mu\gamma^*}^{NP}(p, W, Q^2) \\ &+ \sum_{i=1}^{i_{\max}} \frac{\gamma_{\mu;i}^a(p) \gamma_{\gamma^*;i}^c(W, Q^2)}{W - m_i^b}, \end{aligned} \quad (2.5)$$

introducing the Q^2 -dependence via a separable ansatz,

$$\begin{aligned} \alpha_{\mu\gamma^*}^{NP}(p, W, Q^2) &= \tilde{F}_{\mu}(Q^2) \alpha_{\mu\gamma}^{NP}(p, W), \\ \gamma_{\gamma^*;i}^c(W, Q^2) &= \tilde{F}_i(Q^2) \gamma_{\gamma^*;i}^c(W). \end{aligned} \quad (2.6)$$

The Q^2 -independent pieces on the right-hand side of both equations represent the input from the JüBo2017 solution [85]. Specifically, $\gamma_{\gamma^*;i}^c$ describes the interaction of the photon with the resonance state i with bare mass m_i^b and $\alpha_{\mu\gamma}^{NP}$ accounts for the coupling of the photon to the so-called background or non-pole part of the amplitude. Both quantities are parameterized by energy-dependent polynomials, see Ref. [9].

The Q^2 -dependence is encoded entirely in the channel-dependent form-factor $\tilde{F}_{\mu}(Q^2)$ and another channel-independent form-factor $\tilde{F}_i(Q^2)$ that depends on the resonance index i . We emphasize that this structure is inherited from the JüBo photoproduction ansatz, which separates the photon-induced vertex (γ^c) from the decay vertex of an s-channel resonance to the meson-baryon pair (γ_{μ}^a). Both $\tilde{F}_{\mu}(Q^2)$ and $\tilde{F}_i(Q^2)$ are chosen as

$$\begin{aligned} \tilde{F}_{\mu}(Q^2) &= \tilde{F}_D(Q^2) e^{-\beta_{\mu}^0 Q^2/m^2} P^N(Q^2/m^2, \vec{\beta}_{\mu}), \\ \tilde{F}_i(Q^2) &= \tilde{F}_D(Q^2) e^{-\delta_i^0 Q^2/m^2} P^N(Q^2/m^2, \vec{\delta}_i), \end{aligned} \quad (2.7)$$

where $P^N(x, \vec{y}) = 1 + xy_1 + \dots + x^N y_N$ is a general polynomial with free parameters to be fitted together with δ_i^0 and β_{μ}^0 to the electroproduction data. The parameter-free form factor $\tilde{F}_D(Q^2)$ encodes the empirical dipole behavior, usually implemented in such problems, as well as

a Woods-Saxon form factor which ensures suppression at large Q^2 . It reads

$$\tilde{F}_D(Q^2) = \frac{1}{(1 + Q^2/b^2)^2} \frac{1 + e^{-Q_r^2/Q_w^2}}{1 + e^{(Q^2 - Q_r^2)/Q_w^2}} \quad (2.8)$$

with $b^2 = 0.71 \text{ GeV}^2$, $Q_w^2 = 0.5 \text{ GeV}^2$ and $Q_r^2 = 10.0 \text{ GeV}^2$, see Ref. [82] for more details. Note that we have increased the range parameter Q_r^2 , such that the suppression from the Wood-Saxon form factor is only relevant beyond the range of data considered here ($Q^2 > 8 \text{ GeV}^2$).

As stated above, this procedure relies heavily on the input from the photoproduction, i.e., the functions $\alpha_{\mu\gamma}^{NP}(p, W)$ and $\gamma_{\gamma^*i}^c(W)$. This input does not exist for the longitudinal multipoles as their contribution vanishes exactly at the photon-point. In this case we employ a strategy similar to that of Ref. [65]:

1) We recall that at the *pseudo-threshold* ($q = 0$) the electric and longitudinal multipoles are related according to Siegert's condition [129, 130] as

$$\left. \frac{E_{\ell+}}{L_{\ell+}} \right|_{q=0} = 1, \quad \left. \frac{E_{\ell-}}{L_{\ell-}} \right|_{q=0} = \frac{\ell}{1 - \ell}. \quad (2.9)$$

For more details, see Sec. 2.2-2.3 of Ref. [65], or the earlier derivations in Refs. [126, 130]. Therefore, we apply at the nearest pseudo-threshold point, $Q_{\text{PT}}^2 = -(W - m)^2$,

$$\alpha_{\mu\gamma^*}^{NP, L\ell\pm}(p, W, Q^2) = \frac{\omega}{\omega_{\text{PT}}} \frac{\tilde{F}_D(Q^2)}{\tilde{F}_D(Q_{\text{PT}}^2)} \quad (2.10)$$

$$\times D_{\mu}^{\ell\pm}(W, Q^2) \alpha_{\mu\gamma^*}^{NP, E\ell\pm}(p, W, Q_{\text{PT}}^2),$$

and

$$\gamma_{\gamma^*i}^{c, L\ell\pm}(W, Q^2) = \frac{\omega}{\omega_{\text{PT}}} \frac{\tilde{F}_D(Q^2)}{\tilde{F}_D(Q_{\text{PT}}^2)} \quad (2.11)$$

$$\times \tilde{D}_i^{\ell\pm}(W, Q^2) \gamma_{\gamma^*i}^{c, E\ell\pm}(W, Q_{\text{PT}}^2).$$

The photon energy is $\omega_{\text{PT}} = (W^2 - m^2 - Q_{\text{PT}}^2)/(2W)$. The new functions $D^{\ell\pm}(Q^2)$ ensure Siegert's condition and a consistent falloff behavior in Q^2 as

$$D_{\mu}^{\ell+}(W, Q^2) = e^{-\beta_{\mu}^0 q/q_{\gamma}} P^N(q/q_{\gamma}, \vec{\beta}_{\mu}), \quad (2.12)$$

$$\tilde{D}_i^{\ell+}(W, Q^2) = e^{-\delta_i^0 q/q_{\gamma}} P^N(q/q_{\gamma}, \vec{\delta}_i),$$

$$D_{\mu}^{\ell-}(W, Q^2) = -\frac{\ell-1}{\ell} e^{-\beta_{\mu}^0 q/q_{\gamma}} P^N(q/q_{\gamma}, \vec{\beta}_{\mu}),$$

$$\tilde{D}_i^{\ell-}(W, Q^2) = -\frac{\ell-1}{\ell} e^{-\delta_i^0 q/q_{\gamma}} P^N(q/q_{\gamma}, \vec{\delta}_i),$$

respectively, to the pole and non-pole part for $q_{\gamma} = q(Q^2 = 0)$.

2) In two specific cases ($(\ell\pm, I) = (1-, 1/2)$ and $(\ell\pm, I) = (1-, 3/2)$) the electric multipole vanishes due to selection rules, rendering the implementation of Siegert's theorem nonsensical. In these cases, we decided

to obtain the longitudinal multipole from the magnetic one using a new real-valued normalization constants ζ^{NP} to be determined from the fit,

$$\alpha_{\mu\gamma^*}^{NP, L\ell\pm}(p, W, Q^2) = \zeta_{\mu}^{NP} \frac{\omega}{\omega_{\text{PT}}} \tilde{F}^{\mu}(Q^2) \quad (2.13)$$

$$\times \alpha_{\mu\gamma^*}^{NP, M\ell\pm}(p, W),$$

$$\gamma_{\gamma^*i}^{c, L\ell\pm}(W, Q^2) = \zeta_i \frac{\omega}{\omega_{\text{PT}}} \tilde{F}^{\mu}(Q^2) \gamma_{\gamma^*i}^{c, M\ell\pm}(W).$$

Using the magnetic multipole as starting point, and a real-valued normalization constant ensures that Watson's theorem is fulfilled. Before writing down the final relation between the generic multipole functions ($\bar{E}_{\ell\pm}$, $\bar{M}_{\ell\pm}$, $\bar{L}_{\ell\pm}$) and corresponding multipoles, we note that the latter obey a certain behavior at the pseudo- ($q = 0$) and production threshold ($k = 0$),

$$\begin{aligned} \ell \geq 0: \quad & \lim_{k \rightarrow 0} E_{\ell+} = k^{\ell}, & \lim_{q \rightarrow 0} E_{\ell+} = q^{\ell}, \\ \ell \geq 0: \quad & \lim_{k \rightarrow 0} L_{\ell+} = k^{\ell}, & \lim_{q \rightarrow 0} L_{\ell+} = q^{\ell}, \\ & \lim_{k \rightarrow 0} L_{1-} = k, & \lim_{q \rightarrow 0} L_{1-} = q, \\ \ell \geq 1: \quad & \lim_{k \rightarrow 0} M_{\ell\pm} = k^{\ell}, & \lim_{q \rightarrow 0} M_{\ell\pm} = q^{\ell}, \\ \ell \geq 2: \quad & \lim_{k \rightarrow 0} E_{\ell-} = k^{\ell}, & \lim_{q \rightarrow 0} E_{\ell-} = q^{\ell-2}, \\ \ell \geq 2: \quad & \lim_{k \rightarrow 0} L_{\ell-} = k^{\ell}, & \lim_{q \rightarrow 0} L_{\ell-} = q^{\ell-2}. \end{aligned} \quad (2.14)$$

We incorporate these conditions using

$$\mathcal{M}_{\mu\gamma^*}(k, W, Q^2) = R_{\ell'}(\lambda, q/q_{\gamma}) \bar{\mathcal{M}}_{\mu\gamma^*}(k, W, Q^2) \quad (2.15)$$

for each multipole type and total angular momentum individually. Here,

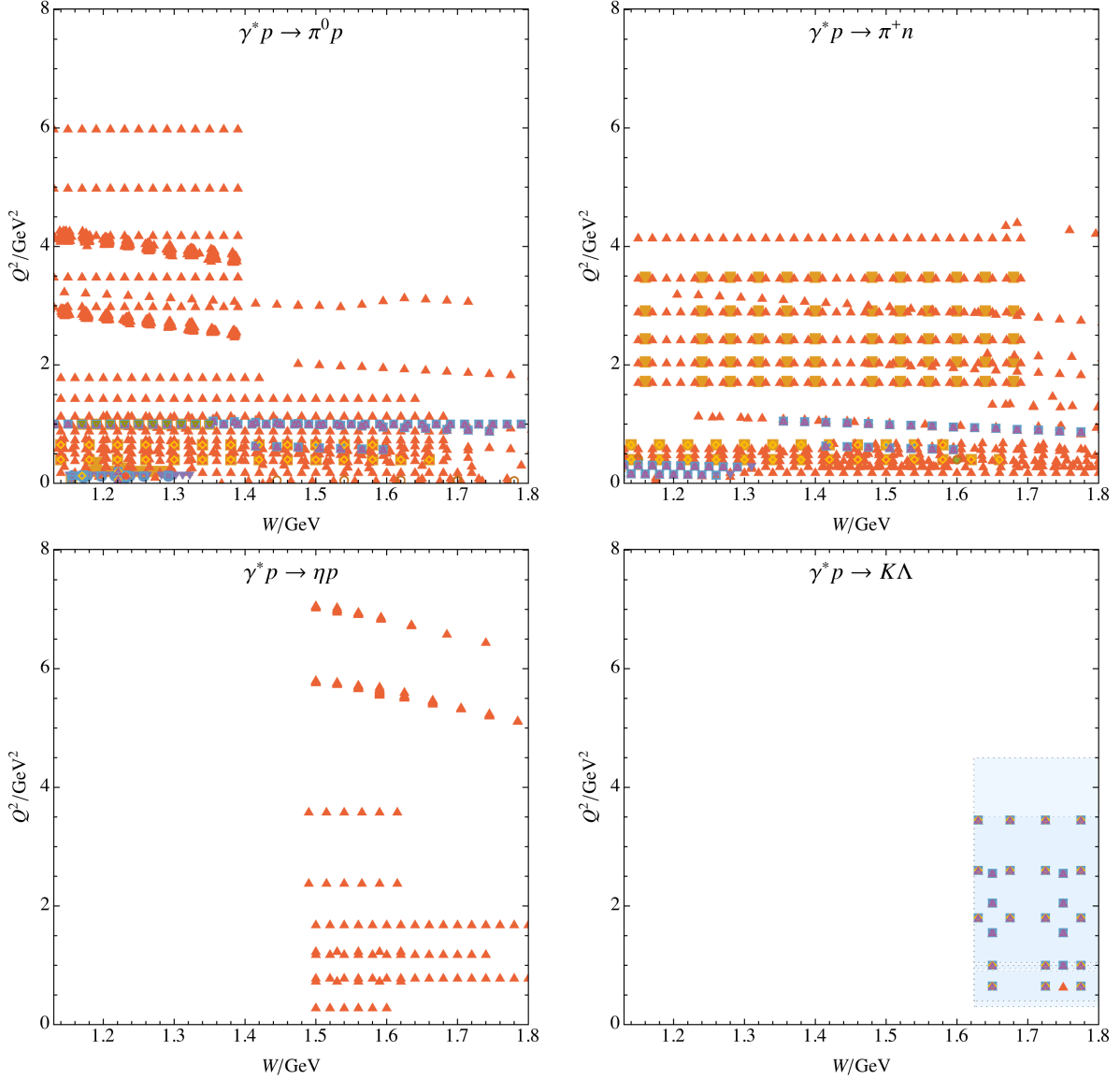
$$R_{\ell'}(\lambda, r) = \frac{B_{\ell'}(\lambda r)}{B_{\ell'}(\lambda)} \quad (2.16)$$

$$\text{with } \ell' = \begin{cases} \ell, & \text{for } E_{\ell+}, L_{\ell\pm}, M_{\ell\pm}, \\ \ell - 2, & \text{for } E_{\ell-}, L_{\ell-} \text{ and } \ell \geq 2, \end{cases}$$

in terms of the Blatt-Weisskopf barrier-penetration factors [188, 189],

$$\begin{aligned} B_0(r) &= 1, \\ B_1(r) &= r/\sqrt{1+r^2}, \\ B_2(r) &= r^2/\sqrt{9+3r^2+r^4}, \\ B_3(r) &= r^3/\sqrt{225+45r^2+6r^4+r^6}, \\ B_4(r) &= r^4/\sqrt{11025+1575r^2+135r^4+10r^6+r^8}. \end{aligned} \quad (2.17)$$

The new free parameters λ need to be determined from a fit to the data. For simplicity and to keep the number of parameters low, the λ s are chosen as channel-independent. Note that one could further try to use baryon chiral perturbation theory to constrain the amplitudes at low momenta and energies, however, the framework for doing that has not been worked out in all necessary details [47].



Type	$N_{\text{data}}^{\pi^0 p}$	$N_{\text{data}}^{\pi^+ n}$	$N_{\text{data}}^{\eta p}$	$N_{\text{data}}^{K\Lambda}$
\bullet ρ_{LT}	45 [131, 132]	—	—	—
\blacksquare $\rho_{LT'}$	2768 [133–137]	5068 [138, 139]	—	—
\blacklozenge σ_L	—	2 [140]	—	—
\blacktriangle $d\sigma/d\Omega$	48135 [134, 135, 141–162]	44266 [139, 146, 161, 163–175]	3665 [176–179]	2055 [180, 181]
\blacktriangledown $\sigma_T + \epsilon\sigma_L$	384 [131, 134, 141, 155, 156, 182–184]	182 [164, 169]	—	204 [180, 181]
\circ σ_T	30 [159]	2 [140]	—	—
\square σ_{LT}	373 [131, 134, 141, 155, 156, 182–184]	138 [164, 169]	—	204 [180, 181]
\diamond $\sigma_{LT'}$	214 [133, 155, 182, 183]	208 [133]	—	156 [180, 185]
\triangle σ_{TT}	327 [141, 155, 156, 183, 184]	123 [164, 169]	—	204 [180, 181]
\blacktriangledown K_{D1}	1527 [135]	—	—	—
\bullet P_Y	—	2 [186, 187]	—	—
Total	53804	49989	3665	2823

FIG. 2. Overview over the fit ranges and data types used in this work. The kinematical region covered by the recent beam-recoil transferred polarization measurement of Ref. [122] is represented by the blue shaded area. These data are not part of the fits but is discussed in Sec. IV.

In summary, for every partial wave, the multipoles E^μ , M^μ and L^μ are fully determined up to: (1) $(1 + N)$ channel-dependent fit parameters $\beta_\mu^0, \dots, \beta_\mu^N$ for the non-pole part; (2) $(1 + N)$ channel-independent parameters $\delta_i^0, \dots, \delta_i^N$ for each of the i_{\max} resonances; (3) one channel-independent threshold behavior regulating parameter λ ; (4) channel-(in)dependent normalization factors $\zeta_\mu^{NP}(\zeta_i)$. Finally, any observable can be constructed from the described multipoles using a standard procedure involving CGLN and helicity amplitudes [123]. For explicit formulas we refer the reader to the previous publication [82].

III. DATA AND FITS

In the present approach we extend the partial-wave basis to S-, P-, D- and F-waves which is necessary having extended the maximal energy range $W_{\max} = 1.6 \mapsto 1.8$ GeV with respect to the previous works [82, 83]. Including then all parameters for $\pi N, \eta N, K\Lambda$ channels, while limiting $N = 2$, and fixing $\zeta_{\mu \neq \eta N, K\Lambda}^{NP} \equiv \zeta_{\pi N}^{NP}$ as well as $\beta_{\mu \notin \{\pi N, \eta N, K\Lambda\}}^{i \in \{0,1,2\}} = 0$ we obtain 533 free parameters of the model. These parameters are fixed to the database consisting of $N_{\text{data}} = 110281$ data as presented in Fig. 2. Specifically, covered are all available electroproduction data as of 2022 in the energy region $W \in [1.13, 1.8]$ GeV and $Q^2 \in (0, 8]$ GeV² for the

$$\aleph = \{\pi^0 p, \pi^+ n, \eta p, K^+ \Lambda\}$$

final states. The data base covers 11 types of observables, see Fig. 2 and Ref. [82] for explicit expressions in terms of the multipoles $\{E, M, L\}$. In previous fits [82, 83] the respective solutions were used to identify many outliers due to typos in older data bases, which are cleaned up in this version and are also available through the JBW web-page [91].

Fits were performed utilizing high-performance computing resources at The George Washington University [190]. In that, the MINUIT library was used to minimize either the regular (unweighted) χ^2 -function

$$\chi^2 = \sum_{i=1}^{N_{\text{all}}} \left(\frac{O_i^{\text{exp}} - O_i}{\Delta_i^{\text{stat}} + \Delta_i^{\text{syst}}} \right)^2, \quad (3.1)$$

or, taking into account the very different number of data points in the πN channels of order $\mathcal{O}(10^5)$ to those in $K\Lambda$ or ηN channels of order $\mathcal{O}(10^3)$, the weighted χ^2 -function

$$\chi_{\text{wt}}^2 = \sum_{j \in \aleph} \frac{N_{\text{all}}}{4N_j} \sum_{i=1}^{N_j} \left(\frac{O_{ji}^{\text{exp}} - O_{ji}}{\Delta_{ji}^{\text{stat}} + \Delta_{ji}^{\text{syst}}} \right)^2, \quad (3.2)$$

where N_j is the number of data for a given final state j . In both of these cases, statistical and systematic uncertainties have been added linearly. We note that while this is only one possible choice, the available data base is quite heterogeneous and has consistency issues, some examples of which were discussed in Ref. [83].

	χ_{dof}^2	$\chi_{\text{pp}}^2(\pi^0 p)$	$\chi_{\text{pp}}^2(\pi^+ n)$	$\chi_{\text{pp}}^2(\eta p)$	$\chi_{\text{pp}}^2(K^+ \Lambda)$
FIT₁	1.42	1.40	1.47	1.49	0.70
FIT₂	1.35	1.38	1.35	1.40	0.58
	$\chi_{\text{wt, dof}}^2$	$\chi_{\text{pp}}^2(\pi^0 p)$	$\chi_{\text{pp}}^2(\pi^+ n)$	$\chi_{\text{pp}}^2(\eta p)$	$\chi_{\text{pp}}^2(K^+ \Lambda)$
FIT₃	1.12	1.44	1.61	1.08	0.33
FIT₄	1.06	1.42	1.44	1.09	0.32

TABLE I. Fit results of the present analysis with respect to standard (3.1) and weighted (3.2) ('wt') χ^2 functions. The last four columns separate out contributions for individual final-state channels (χ^2 per datum) for convenience.

Using different parameter sets determined in Ref. [83] as starting values and different strategies we found two local minima for each version of the χ^2 -function. The results are quoted in Tab. I.

We observe that all four solutions lead to a similar data description with the weighted solutions (**FIT₃**, **FIT₄**) improving the ηN and $K\Lambda$ data description. This is indeed expected as those data have more weight in these fits. In Fig. 3 we also show the χ^2 for each data point color-coded for the three data references. The curves correspond to **FIT₁**, representative for all four solutions. The most modern (2013, orange) data [180] are described consistently better than the slightly older data from Ref. [181] (blue) and Ref. [185] (green).

Furthermore, throughout all four solutions of the present analysis, we observe that the largest contributions to the χ^2 indeed come from low- Q^2 and low- W values. This is visualized in the top panel of Fig. 4. Comparing this with the data representation of Fig. 2 the observed accumulation at low Q^2 and W corresponds to the fact that most data are measured in that region. Still, one can also conclude that more data in the large Q^2 region would be very desirable. Normalizing the same binned (in W and Q^2) χ^2 distribution we obtain the bottom panels of Fig. 4. Discrepancies are mostly observed at higher energies, which could be a sign that G-waves become important. Also, there is a large discrepancy at $W \sim 1.6$ GeV and large Q^2 that comes from the difficulty to describe the ηN electroproduction data [179] in that region. In our previous analysis [83] the data was not included due to the restricted Q^2 range, but now the large contribution to the χ^2 shows that the asymptotic Q^2 behavior might need to be explored further in future updates of the model. In any case, **FIT₃** and 4 perform quite well in that region.

IV. DISCUSSION

This work is the next step on the quest of uniting the description of meson-, real photon- and virtual photon-induced reactions through the dynamical coupled-channel approach. In that, several theoretical challenges have been overcome, such as including higher partial-waves (up to F-waves), extending the parameterization to independent Q^2 -parameterization in the

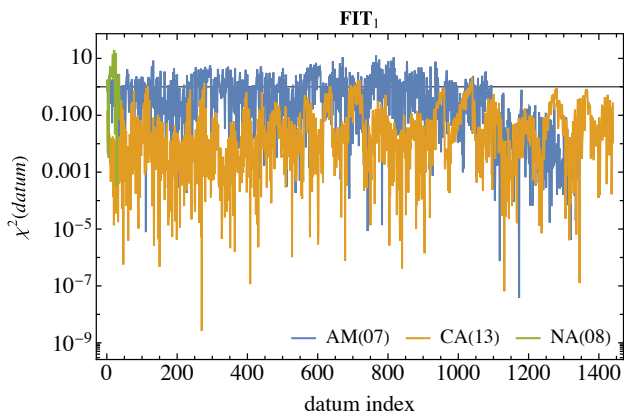


FIG. 3. Distribution of partial χ^2 values per datum for the $K^+\Lambda$ final states, for **FIT**₁. Data is taken from CA(13) [180], AM(07) [181] NA(08) [185].

$K\Lambda$ channels, extending the kinematic range and, consequently, the data base.

As a first step it is useful to examine the photoproduction solution which is used as input for the current analysis, i.e., JüBo2017 [85]. A comparison of this to other available solutions such as Bonn-Gatchina 2019 [191] or KAON-MAID [110, 192] is depicted for some representative multipoles in Fig. 5. We observe larger deviations between the models compared to the case of ηN final states (see Fig. 2 in Ref. [83]). The reason is that the approaches are parametrized differently. In addition, existing data in photoproduction are not complete to uniquely pin down multipoles up to a global phase, and JüBo and Bonn-Gatchina fit slightly different data bases. However, except for KAON-MAID, the approaches describe the bulk of modern cross section and polarization data to a very comparable accuracy.

Turning now to non-vanishing virtuality, we note first that the description of the πN electroproduction channels improved in the present study, irrespective of the utilized form of the χ^2 -function, according to $\chi_{\text{dof}}^2 \approx (1.7 \rightarrow 1.4)$ comparing to previous πN and $\pi N/\eta N$ analyses [82, 83]. The obvious reason for this is the increased number of free-parameters due to the $K\Lambda$ channel, and inclusion of higher partial waves. Still, this observation is non-trivial as the number of included data has been increased as well, covering a larger kinematic range. Being more specific, we compare the estimated multipoles with those of the previous solution [83], where only S-/P-/D-waves and $\pi N/\eta N$ data in the range $W < 1.6$ GeV were included. We find that both πN and ηN channels agree with the previous results while the discrepancy among the multipoles across the four different solutions seems to have been reduced in the new result. As an explicit example, we show in the appendix (see Fig. 12 and Fig. 13) the Q^2 behaviour of the πN and ηN multipoles projected to isospin $I = 1/2$ for fixed total energy $W = 1.535$ GeV. This is to be compared with the Fig. 7 in Ref. [83]. We note, that the reduction of the differences between mul-

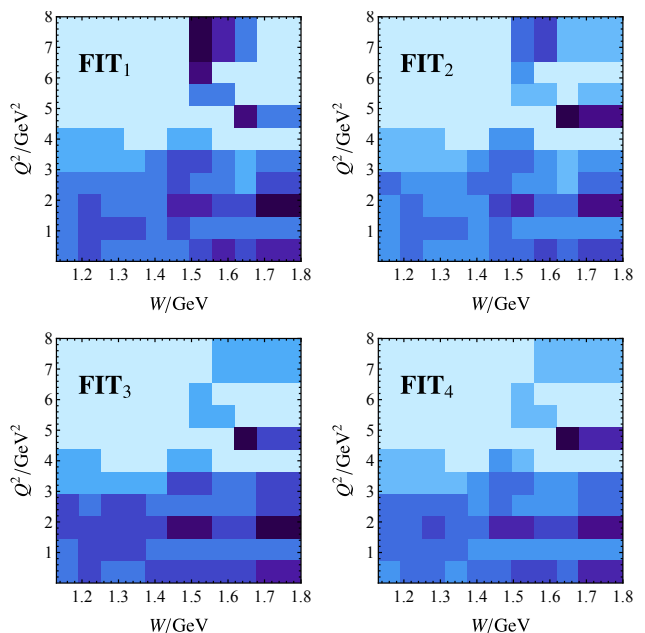
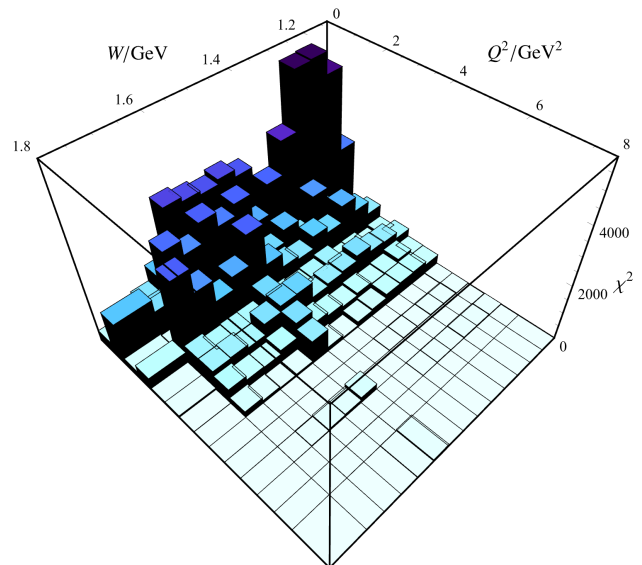


FIG. 4. Distribution of χ^2 . Top: Binned distribution of total $\chi^2(W, Q^2)$ for a typical solution, here **FIT**₁. Bottom: Binned distribution of $\chi^2(W, Q^2)$ weighted per number of points in each (W, Q^2) bin. Shades of blue correspond to the linearly scaled range of values [0.0, 4.0].

tipoles is somewhat indicative at this point due to the so far incomplete error-analysis, but it does make sense as much more data have now been included into the data base. A similar behavior was found in the context of Chiral Unitary Models: In Ref. [193] the first NNLO analysis was performed that has a substantially larger number of parameters than at NLO. However, it was also the first analysis to include data from all strangeness sectors $S = -1, 0, +1$ in meson-baryon dynamics simultaneously. As a result, the uncertainties of resonance pole positions were reduced, compared to NLO analyses, despite the

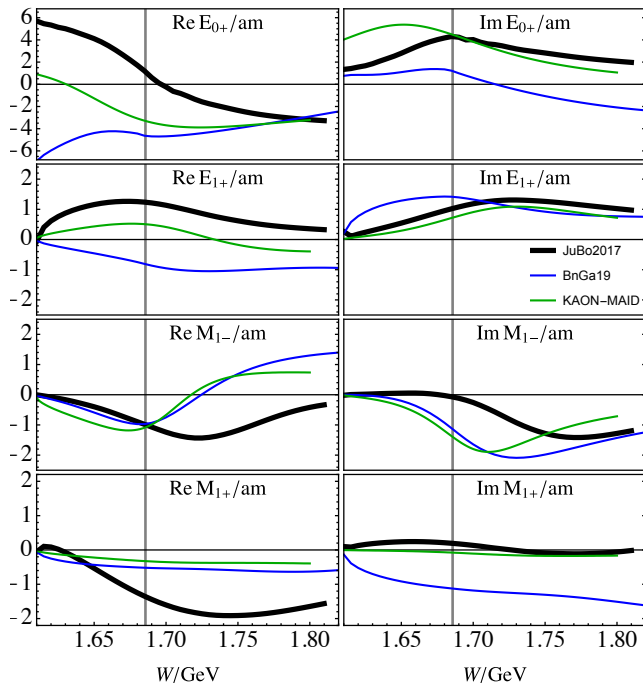


FIG. 5. Model input in the $K^+\Lambda$ final state at the photo point $Q^2 = 0 \text{ GeV}^2$ provided by the JüBo2017 solution [85] (black lines) compared to the Bonn-Gatchina 2019 analysis [191] (blue) and KAON-MAID [110, 192] (green, multiplied by (-1) because of the different conventions). The vertical lines show the position of the $K\Sigma$ threshold while am refers to mfm.

larger number of fit parameters.

Multipoles projected to the $K^+\Lambda$ final state are depicted in Fig. 6 for fixed $Q^2 = 0.5 \text{ GeV}^2$ and those for a fixed $W = 1.7 \text{ GeV}$ in Fig. 7. Results at other kinematics can be obtained from JBW web page. In these figures we also make a comparison with the results of the KAON-MAID [110] study. One notes directly, that agreement to this analysis can be found only in few single cases or in very restricted kinematical ranges even when taking into account possible phase convention difference between JBW and KAON-MAID. Still, it has to be noted that KAON-MAID was only fitted to a very limited subset of today's electroproduction data and should, thus, be taken with a grain of salt. In particular, it seems that the phenomenology of the KAON-MAID solutions necessarily leads to very large longitudinal multipoles. As it will be discussed below, this will have some important consequence when addressing new polarisation transfer data [122] from the CLAS collaboration.

Comparing our obtained solutions among each other and also to the available KAON-MAID [110] results (see, e.g., Fig. 6) we note large theoretical uncertainty in several multipoles. In the present, largely data-driven, approach this uncertainty simply reflects the lack of data in certain kinematical regions as well as their incompleteness regarding the so-called complete experiment [80, 81].

To investigate this volatility in a more quantitative way, we define the following procedure, similar to what was proposed for the photoproduction case in Ref. [194]. First the kinematic range $(W/\text{GeV}, Q^2/\text{GeV}^2) \in ([1.13, 1.8], (0, 8])$ is split up in bins. Then for each (W, Q^2) bin a modified variance of all four obtained solutions ($i = 1, \dots, 4$) is calculated as

$$\overline{\text{Var}}(W, Q^2)(X) := \sum_{\ell \pm} \frac{\text{Var}\{|X_{\ell \pm, i}|\}}{\text{Mean}\{|X_{\ell \pm, i}|\} + \varepsilon}, \quad (4.1)$$

where $X \in \{E, M, L\}$ denotes the considered multipole type and $\varepsilon = 10^{-3} \text{ am}$ is a regulator to avoid division by zero in certain cases. The result is shown for all multipoles separately in the top row of Fig. 8. We observe that the electric multipole is constrained quite well in nearly all kinematic regions with the highest uncertainty provided in the threshold region at moderate Q^2 . The magnetic multipole is unrestricted only for high Q^2 values. The volatility of electric and magnetic multipoles is, however, dwarfed by that of the longitudinal multipole. Indeed, it shows large volatility in all kinematic regions except of a $1 \lesssim Q^2/\text{GeV}^2 \lesssim 3$ valley. This maybe because of the availability of the experimental data on the $K^+\Lambda$, see Fig. 2. Combined together $\overline{\text{Var}}(E, M, L) := \overline{\text{Var}}(E) + \overline{\text{Var}}(M) + \overline{\text{Var}}(L)$ the aggregated measure of volatility is provided in the bottom part of the Fig. 8. It shows clearly that it is dominated by the uncertainty in the longitudinal multipole where the most uncertain kinematic regions are those of low Q^2 and those of higher Q^2 . This can be directly related to the poor data situation in this region, emphasizing again the importance of the high-virtually experimental programs such as CLAS12 [73, 122] or the EIC [195, 196].

Having quantified that the largest uncertainties are due to the longitudinal multipoles, we proceed by calculating observables which are sensitive to these multipoles. Of particular importance is the so-called beam-recoil transferred polarization $\{P'_a | a = (x', z')\}$ for the Cartesian coordinate components (x', y', z') , such that the $e_{z'}$ is aligned with the outgoing K^+ and the $e_{y'}$ axis is normal to the reaction plane, see Fig. 1. The corresponding quantities for the scattering plane (components (x, y, z)) lead to $\{P'_a | a = (x, z)\}$ observables, see Ref. [122] for more details on measurement techniques and observable definitions. So far many of these data have been taken by the CLAS/CLAS12 collaboration [122, 197, 198], while we will refer to the most recent data [122] from CLAS12. As such these data were taken at integrated kinematics such that $P'_a(W, Q^2, \cos \theta, E_e)$ is available over extended bins in one or two kinematic variables. In terms of quantities defined in the present work these *integrated* observ-

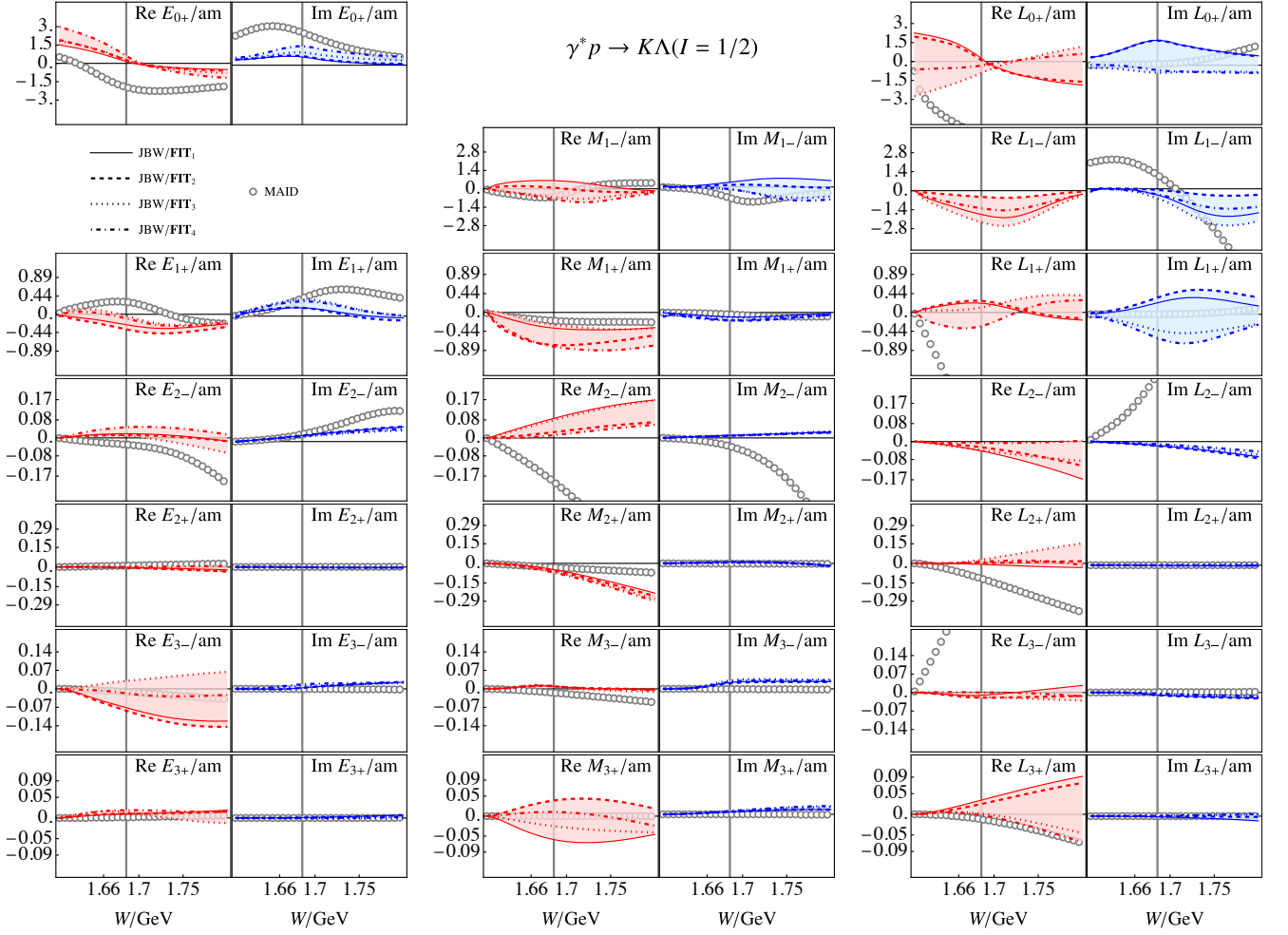


FIG. 6. JBW-multipoles for the $K\Lambda(I = 1/2)$ final state. Different solutions are denoted by JBW/**FIT**_{1..4} (connected by shading to guide the eye), while circles represent the KAON-MAID [110] solution (multiplied by (-1)). Results are separated w.r.t. type, angular momentum, real and imaginary parts, and are shown for a fixed value of photon virtuality $Q^2 = 0.5 \text{ GeV}^2$. Results for other kinematics can be obtained from the JBW web page <https://jbw.phys.gwu.edu>. The vertical lines shows the position of the $K\Sigma$ threshold.

ables are defined as

$$P'_{x'}(W, E_e) = \frac{1}{\mathcal{N}} \int_{-1}^{+1} dc \int_{Q_{\min}^2}^{Q_{\max}^2} dQ^2 K \sqrt{1 - \epsilon^2} R_{TT'}^{x'0}, \quad (4.2)$$

$$P'_{z'}(W, E_e) = \frac{1}{\mathcal{N}} \int_{-1}^{+1} dc \int_{Q_{\min}^2}^{Q_{\max}^2} dQ^2 K \sqrt{1 - \epsilon^2} R_{TT'}^{z'0}, \quad (4.3)$$

$$P'_x(W, E_e) = \frac{1}{\mathcal{N}} \int_{-1}^{+1} dc \int_{Q_{\min}^2}^{Q_{\max}^2} dQ^2 K \frac{\sqrt{\epsilon(1 - \epsilon)}}{2} \left(R_{LT'}^{x'0} c - R_{LT'}^{y'0} + R_{LT'}^{z'0} s \right), \quad (4.4)$$

$$P'_z(W, E_e) = \frac{1}{\mathcal{N}} \int_{-1}^{+1} dc \int_{Q_{\min}^2}^{Q_{\max}^2} dQ^2 K \sqrt{1 - \epsilon^2} \left(-R_{TT'}^{x'0} s + R_{TT'}^{z'0} c \right), \quad (4.5)$$

$$\mathcal{N} = \int_{-1}^{+1} dc \int_{Q_{\min}^2}^{Q_{\max}^2} dQ^2 K (R_T^{00} + \epsilon R_L^{00})$$

where $c := \cos\theta$, $s := \sin\theta$, $K := k'_i/q(Q^2 = 0)$, while all response functions ($R_{\cdot\cdot}$) are functions of (Q^2, W, c) . Explicit form of these in terms of the multipoles can be found in Ref. [83]. Note that the beam energy E_e enters the right-hand side of the equations through $\epsilon(W, Q^2, E_e)$ defined in Eq. (2.3). The two values of E_e from the Ref. [122] measurements will be considered in the following, namely $E_e = 6.535 \text{ GeV}$ and $E_e = 7.546 \text{ GeV}$, for which the integration limits are provided as $[Q_{\min}^2, Q_{\max}^2] = [0.3, 3.5] \text{ GeV}^2$ and $[Q_{\min}^2, Q_{\max}^2] = [0.4, 4.5] \text{ GeV}^2$, respectively. For these two cases and using all of our four solutions we postdict the results of the integrated quantities $P'_{\cdot\cdot}(W, E_e)$, comparing them with the experimental results in Fig. 9. We observe that some agreement with the data can be seen in P'_x and $P'_{z'}$, irrespectively of the beam energy. The JBW postdictions of $P'_{x'}$ and P'_z are, however, much smaller in the considered kinematic domain compared to the data, and they are

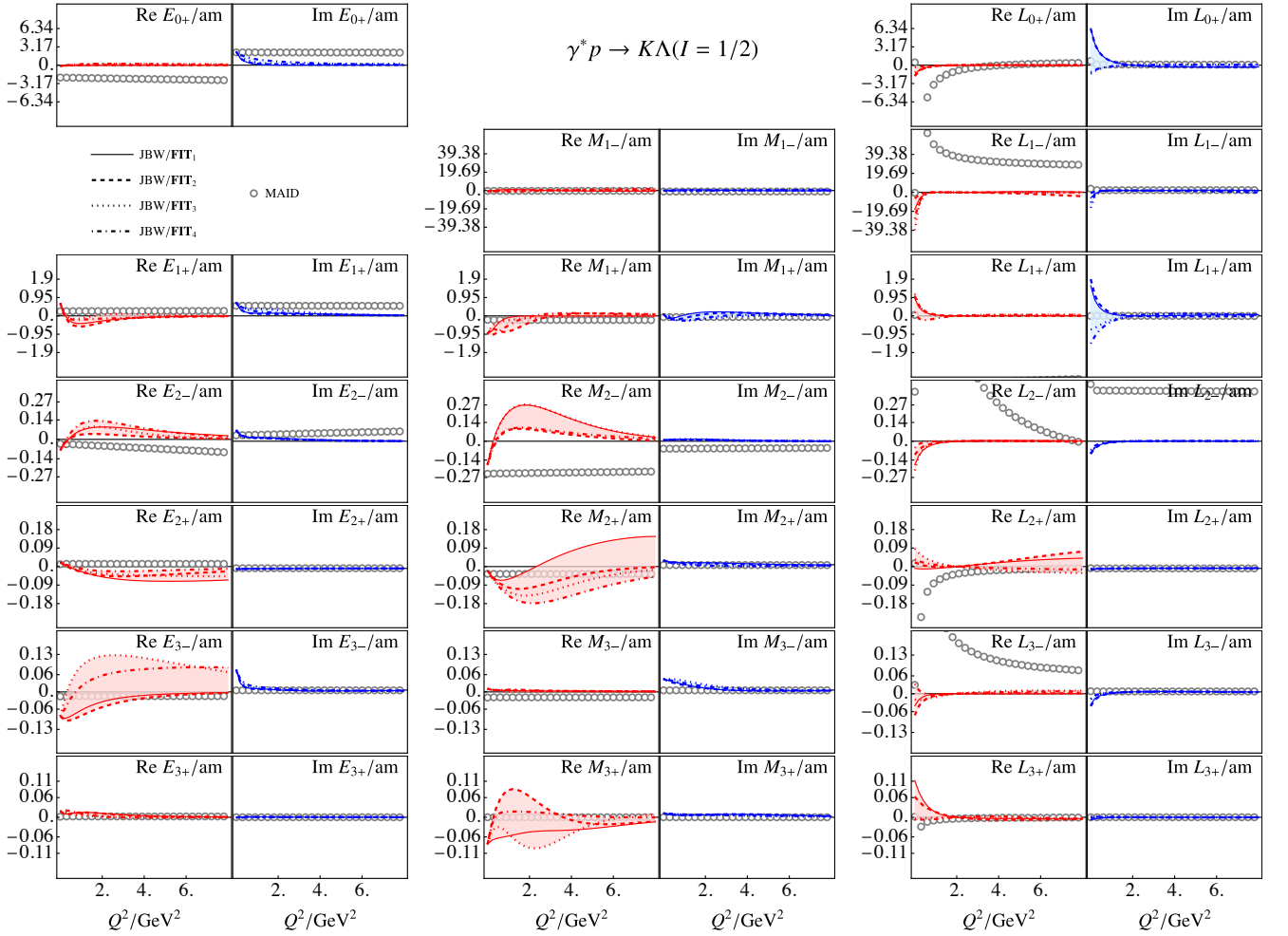


FIG. 7. Multipoles for the $K\Lambda(I = 1/2)$ final state obtained through the JBW coupled-channel analysis of electroproduction data in the $\pi N, \eta N, K\Lambda$ channels. Total energy is fixed to $W = 1.7$ GeV, different solutions are denoted by JBW/**FIT**_{1..4} (connected by shading to guide the eye), results of KAON-MAID [110] are depicted by gray circles (multiplied by (-1)). Results at other kinematics can be obtained from the JBW web page <https://jbw.phys.gwu.edu>.

also different from the KAON-MAID [110] postdictions.

Following up on the latter discrepancy, we note that the largest differences in KAON-MAID vs. JBW results are indeed apparent for the longitudinal multipoles, see Figs. 6 and 7. In some cases we see an order of magnitude difference in these multipoles. The next question is now, can one identify which of the longitudinal multipoles are responsible for the stark suppression of, e.g., JBW postdicted $P'_{x'}$ values in Fig. 9. To quantify this, we took one typical JBW solution (**FIT**₄) and *a-posteriori* turned off various multipoles, recalculating each time $P'_{x'}$. This is demonstrated in Fig. 10 for $P'_{x'}(Q^2, W = 2.169 \text{ GeV}, \theta = 1.719 \text{ rad}, E_e = 6.535 \text{ GeV})$, where all except the virtuality variables are fixed to reproduce a point where experimental photoproduction data exist. Specifically, $C_{x'}$ was measured in Ref. [199] which is also included into the JüBo database. Identifying $P'_{x'} = -\sqrt{1 - \epsilon^2} C_{x'}$ at $Q^2 = 0$ we indeed recover the experimental result at the photon-point. However, the predicted $P'_{x'}$ quickly goes to

much smaller values when increasing Q^2 which we also observe for the integrated $P'_{x'}$ in Fig. 9. We found that turning off the electric or magnetic multipoles has little effect on this Q^2 behaviour. The longitudinal multipoles – foremost the L_{0+} – can change the Q^2 behavior entirely. We expect, therefore, that including polarization transfer data in a future work will have most significant impact on these multipoles.

Finally, we compare our postdiction on the ratio of longitudinal to transverse structure functions to the experimental determinations. By construction, this ratio is strongly dependent on the longitudinal components of the transition amplitude. Additionally, there are quite a few experimental results [200–203], which have similar (but not equal) kinematics. Still, following Ref. [200] we compile our predictions together with experimental results in Fig. 11. Interestingly, our predictions seem to be well in agreement with the trend provided by the experimental determinations [200–203]. One hast to note,

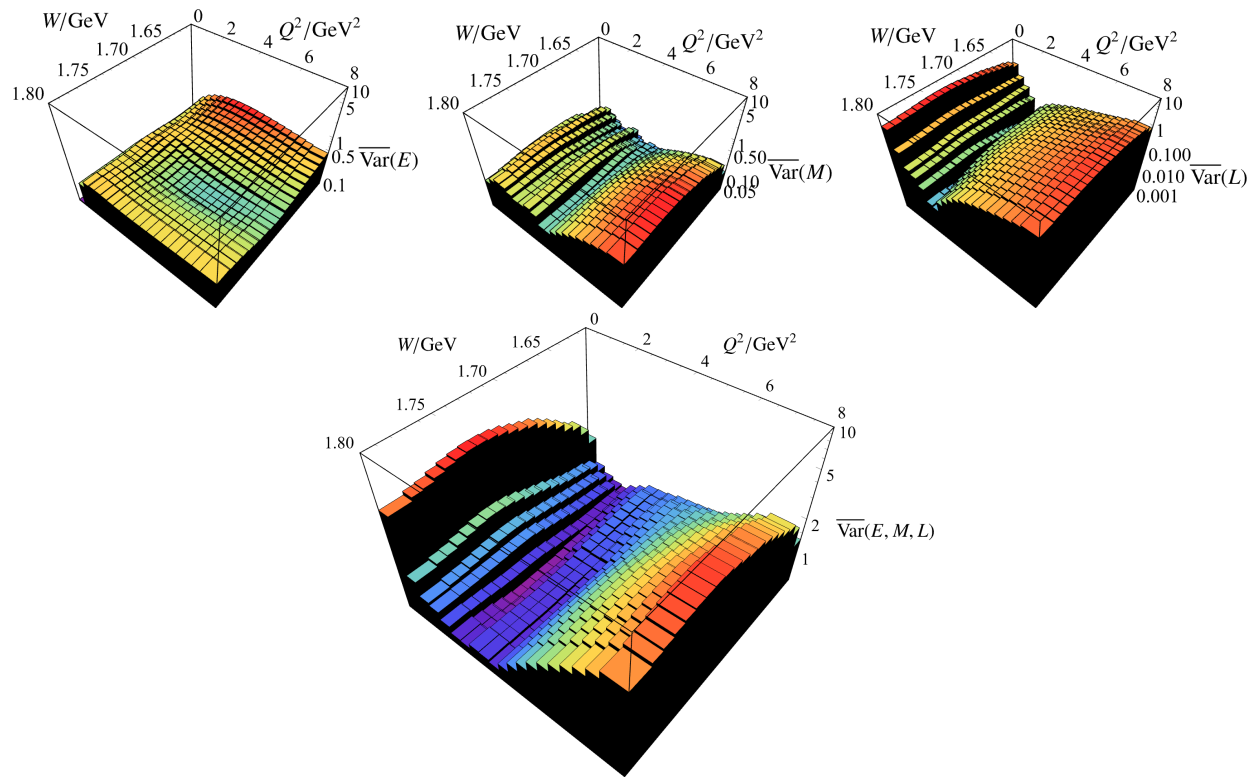


FIG. 8. Systematic uncertainty of the obtained multipoles in the $K^+\Lambda$ channel binned in Q^2 vs. W with respect to individual multipoles $\{E, M, L\}$ aggregated over total angular momentum quantum numbers. For definition of $\overline{\text{Var}}(EML)$ see main text. Bottom figure shows values aggregated additionally over multipole types, i.e., $\overline{\text{Var}}(EML)$.

however, that the data are less precise for this ratio than for the polarization transfer shown in Fig. 9.

V. SUMMARY AND OUTLOOK

In this work a further step has been taken towards providing a unified phenomenology of single-meson pion-induced, photo- and electroproduction data. In that, we have extended our formalism by including up to F-waves; included a new Q^2 parametrization of the $K\Lambda$ channel; extended the data base and range of applicability of our formalism to $W < 1.8$ GeV and $Q^2 < 8$ GeV². Using the multipoles of the JüBo2017 approach at the photon-point ($Q^2 = 0$ GeV²) as constraint to our formalism we fit the Q^2 parameterization to the available experimental data ($N_{\text{data}} \approx 110\,000$).

We find that all three-channels $\{\pi N/\eta N/K\Lambda\}$ are described well. The largest source of uncertainties in the extracted multipoles comes from different local χ^2 minima that we can explore due to an extensive search of the parameter space and different fitting strategies. Also, weighing the data differently in the χ^2 produces large changes in extracted multipoles. This reflects the presence of substantial kinematic gaps in the data to pin down the solution, calling for more measurements. We identify the kinematic regions in which it would be most

valuable to have more data. Discrepancies among extracted multipoles also reflect the presence of ambiguities due to the absence of complete-experiment coverage by different observables. The uncertainties from these sources are much larger than the effects from statistical and systematic errors of the data themselves.

We obtain relatively good χ^2 values for this type of analysis ($\chi^2_{\text{dof}} \approx 1.4$), but, even then, the values are not even close to being acceptable in a statistical sense. This indicates that our 500-parameter fit is not flexible enough and/or there are underestimated inconsistencies in the data base, which is a notorious problem in baryon spectroscopy.

We also observe that the discrepancies become smaller among the extracted $\{\pi N/\eta N\}$ multipoles, corresponding to different local χ^2 minima, when compared to previous studies in which only the $\{\pi N/\eta N\}$ electroproduction channels were fitted. This occurs despite the larger parameter space of the current solution that includes also $K\Lambda$ electroproduction. This behavior is likely a sign that a global analysis indeed provides valuable constraints through coupled-channel effects.

We observe and quantify that the largest uncertainty of our solutions is given by that of the longitudinal multipoles. This means that the available data base consisting in the $K\Lambda$ channel of cross sections only is not restrictive enough for single multipoles. Future progress can

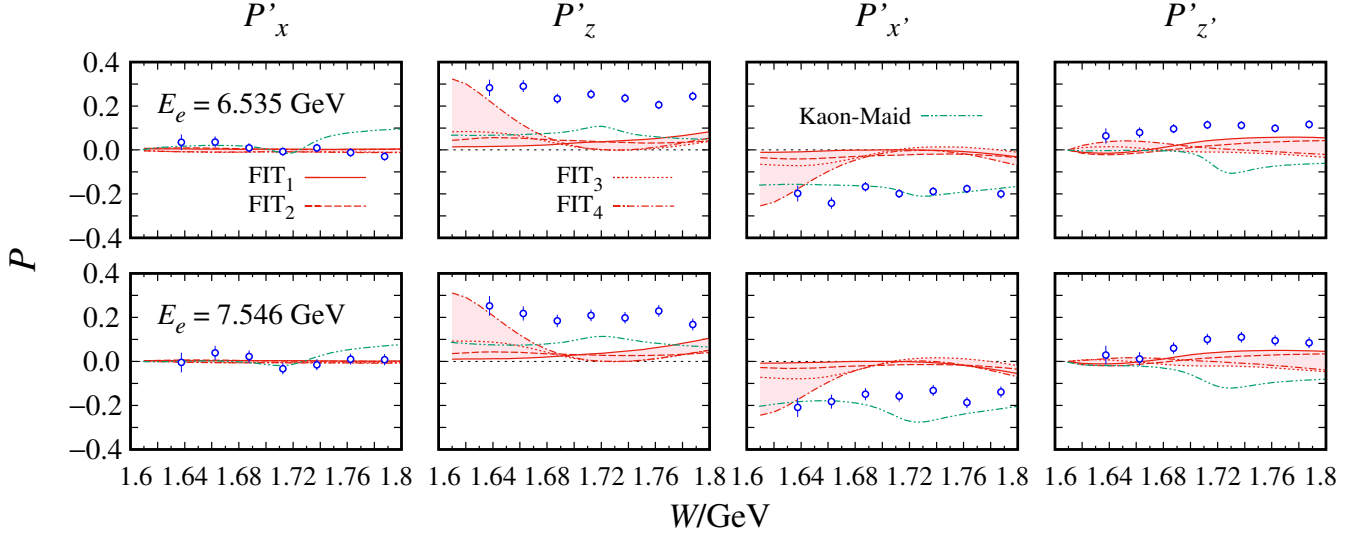


FIG. 9. Transferred Λ polarization components P'_x , P'_z , $P'_{x'}$ and $P'_{z'}$ vs. W for electron beam energies of 6.535 GeV (top panels) and 7.546 GeV (bottom panels). Different solutions denoted by FIT_{1,...,4} (see Tab. 1) are connected by shading to guide the eye, whereas predictions of KAON-MAID are represented by the green dash-dot-dotted lines. Experimental data are taken from Ref. [122].

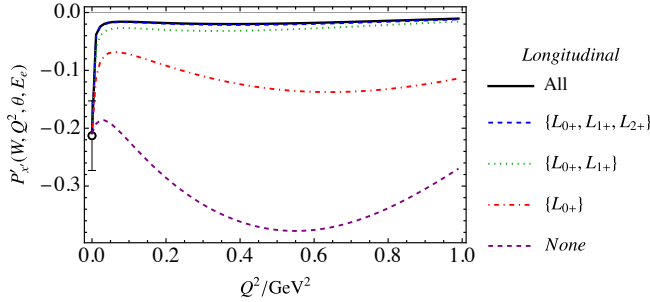


FIG. 10. Polarization transfer as a function of Q^2 for fixed $W = 2.169$ GeV, $E_e = 6.535$ GeV and $\theta = 1.719$ rad. Different lines represent a FIT₄ with a longitudinal multipoles included as specified in the legend. The corresponding experimental data point (black dot) is obtained from Ref. [199] by identifying $P'_{x'} = -\sqrt{1 - \epsilon^2} C_{x'}$ at $Q^2 = 0$.

be achieved by including the recent polarization transfer data measured by the CLAS collaboration. Indeed, we checked that there is some tension between our solutions and available integrated polarization transfer observables. We showcased that low angular momentum longitudinal multipoles are the most crucial contributors to this discrepancy.

We plan to explore the Q^2 -dependence of the $K\Sigma$ channels addressing available experimental data. This will also allow us to consistently include the CLAS polarization-transfer data in the $K\Lambda$ and $K\Sigma$ channels. It is notable that, so far, many of these data are available only in relatively large bins. Thus, an inclusion of such data into the data base would require integrations over some kinematic variables. Measurements with smaller

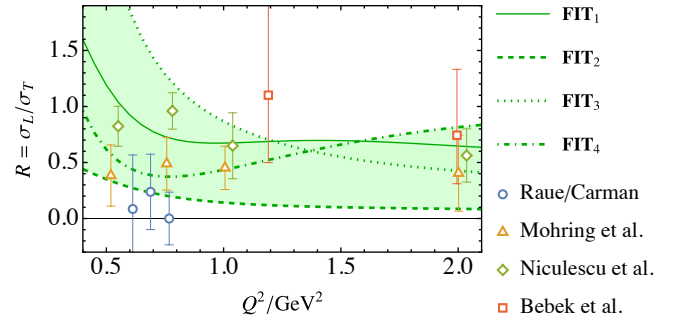


FIG. 11. Ratio of $K\Lambda$ longitudinal to transverse structure functions as a function of Q^2 . Predictions obtained from this work are provided by dark green lines ($\theta = 0$, $W = 1.84$ GeV), connected by the shading to guide the eye. Experimental determinations [200–203] are depicted by empty symbols.

binning are currently on the way by the CLAS collaboration [204]. Finally, the work on extracting helicity couplings of the resonances and the implementation of model selection techniques to produce a more efficient parametrization is ongoing.

Acknowledgements The authors thank Daniel Carman, Viktor Mokeev, and Igor Strakovsky for making data available as well as for inspiring discussions, and DC and VM for a careful reading of the manuscript. The work of MM, UGM and DR was supported in part by the Deutsche Forschungsgemeinschaft (DFG, German Research Foundation) through the funds provided to the Sino-German Collaborative Research Center TRR110 “Symmetries and the Emergence of Struc-

ture in QCD” (DFG Project ID 196253076 - TRR 110). The work of UGM was further supported by the Chinese Academy of Sciences (CAS) President’s International Fellowship Initiative (PIFI) (Grant No. 2018DM0034) and by Volkswagen Stiftung (Grant No. 93562). The work of TM was supported by the PUTI Q2 Grant from University of Indonesia under contract No. NKB-663/UN2.RST/HKP.05.00/2022. The work of MD and

RW was supported in part by the U.S. Department of Energy grant DE-SC0016582; MD’s work was also supported in part by DOE Office of Science, Office of Nuclear Physics under contract DE-AC05-06OR23177. The authors gratefully acknowledge computing time on the supercomputer JURECA [205] at Forschungszentrum Jülich under grant no. “baryonspectro” that was used to produce the input at $Q^2 = 0$.

-
- [1] D. G. Ireland, E. Pasyuk, and I. Strakovsky, Photo-production Reactions and Non-Strange Baryon Spectroscopy, *Prog. Part. Nucl. Phys.* **111**, 103752 (2020), [arXiv:1906.04228 \[nucl-ex\]](#).
- [2] A. Thiel, F. Afzal, and Y. Wunderlich, Light Baryon Spectroscopy, *Prog. Part. Nucl. Phys.* **125**, 103949 (2022), [arXiv:2202.05055 \[nucl-ex\]](#).
- [3] T. Mart, C. Bennhold, and H. Haberzettl, An isobar model for the photoproduction and electroproduction of kaons on the nucleon, *PiN Newslett.* **16**, 86 (2002).
- [4] V. Shklyar, H. Lenske, and U. Mosel, A Coupled-channel analysis of K Lambda production in the nucleon resonance region, *Phys. Rev. C* **72**, 015210 (2005), [arXiv:nucl-th/0505010](#).
- [5] D. Drechsel, S. S. Kamalov, and L. Tiator, Unitary Isobar Model - MAID2007, *Eur. Phys. J. A* **34**, 69 (2007), [arXiv:0710.0306 \[nucl-th\]](#).
- [6] A. V. Anisovich, R. Beck, E. Klempt, V. A. Nikonov, A. V. Sarantsev, and U. Thoma, Properties of baryon resonances from a multichannel partial wave analysis, *Eur. Phys. J. A* **48**, 15 (2012), [arXiv:1112.4937 \[hep-ph\]](#).
- [7] R. L. Workman, M. W. Paris, W. J. Briscoe, and I. I. Strakovsky, Unified Chew-Mandelstam SAID analysis of pion photoproduction data, *Phys. Rev. C* **86**, 015202 (2012), [arXiv:1202.0845 \[hep-ph\]](#).
- [8] H. Kamano, S. X. Nakamura, T. S. H. Lee, and T. Sato, Nucleon resonances within a dynamical coupled-channels model of πN and γN reactions, *Phys. Rev. C* **88**, 035209 (2013), [arXiv:1305.4351 \[nucl-th\]](#).
- [9] D. Rönchen, M. Döring, F. Huang, H. Haberzettl, J. Haidenbauer, C. Hanhart, S. Krewald, U.-G. Meißner, and K. Nakayama, Photocouplings at the Pole from Pion Photoproduction, *Eur. Phys. J. A* **50**, 101 (2014), [Erratum: *Eur.Phys.J.A* 51, 63 (2015)], [arXiv:1401.0634 \[nucl-th\]](#).
- [10] B. C. Hunt and D. M. Manley, Partial-Wave Analysis of $\gamma p \rightarrow K^+ \Lambda$ using a multichannel framework, *Phys. Rev. C* **99**, 055204 (2019), [arXiv:1804.07422 \[nucl-ex\]](#).
- [11] T. Burch, C. Gattlinger, L. Y. Glozman, C. Hagen, D. Hierl, C. B. Lang, and A. Schafer, Excited hadrons on the lattice: Baryons, *Phys. Rev. D* **74**, 014504 (2006), [arXiv:hep-lat/0604019](#).
- [12] J. Bulava, R. G. Edwards, E. Engelson, B. Joo, H.-W. Lin, C. Morningstar, D. G. Richards, and S. J. Wallace, Nucleon, Δ and Ω excited states in $N_f = 2 + 1$ lattice QCD, *Phys. Rev. D* **82**, 014507 (2010), [arXiv:1004.5072 \[hep-lat\]](#).
- [13] G. P. Engel, C. B. Lang, M. Limmer, D. Mohler, and A. Schafer (BGR [Bern-Graz-Regensburg]), Meson and baryon spectrum for QCD with two light dynamical quarks, *Phys. Rev. D* **82**, 034505 (2010), [arXiv:1005.1748 \[hep-lat\]](#).
- [14] R. G. Edwards, J. J. Dudek, D. G. Richards, and S. J. Wallace, Excited state baryon spectroscopy from lattice QCD, *Phys. Rev. D* **84**, 074508 (2011), [arXiv:1104.5152 \[hep-ph\]](#).
- [15] B. J. Menadue, W. Kamleh, D. B. Leinweber, and M. S. Mahub, Isolating the $\Lambda(1405)$ in Lattice QCD, *Phys. Rev. Lett.* **108**, 112001 (2012), [arXiv:1109.6716 \[hep-lat\]](#).
- [16] R. G. Edwards, N. Mathur, D. G. Richards, and S. J. Wallace (Hadron Spectrum), Flavor structure of the excited baryon spectra from lattice QCD, *Phys. Rev. D* **87**, 054506 (2013), [arXiv:1212.5236 \[hep-ph\]](#).
- [17] J. J. Dudek and R. G. Edwards, Hybrid Baryons in QCD, *Phys. Rev. D* **85**, 054016 (2012), [arXiv:1201.2349 \[hep-ph\]](#).
- [18] C. Alexandrou, J. W. Negele, M. Petschlies, A. Strelchenko, and A. Tsapalis, Determination of Δ Resonance Parameters from Lattice QCD, *Phys. Rev. D* **88**, 031501 (2013), [arXiv:1305.6081 \[hep-lat\]](#).
- [19] C. Alexandrou, J. W. Negele, M. Petschlies, A. V. Pochinsky, and S. N. Syritsyn, Study of decuplet baryon resonances from lattice QCD, *Phys. Rev. D* **93**, 114515 (2016), [arXiv:1507.02724 \[hep-lat\]](#).
- [20] F. M. Stokes, W. Kamleh, and D. B. Leinweber, Elastic Form Factors of Nucleon Excitations in Lattice QCD, *Phys. Rev. D* **102**, 014507 (2020), [arXiv:1907.00177 \[hep-lat\]](#).
- [21] G. S. Bali, S. Collins, P. Georg, D. Jenkins, P. Korcyl, A. Schäfer, E. E. Scholz, J. Simeth, W. Söldner, and S. Weishäupl (RQCD), Scale setting and the light baryon spectrum in $N_f = 2 + 1$ QCD with Wilson fermions, *JHEP* **05**, 035, [arXiv:2211.03744 \[hep-lat\]](#).
- [22] M. Ferraris, M. M. Giannini, M. Pizzo, E. Santopinto, and L. Tiator, A Three body force model for the baryon spectrum, *Phys. Lett. B* **364**, 231 (1995).
- [23] L. Y. Glozman and D. O. Riska, The Spectrum of the nucleons and the strange hyperons and chiral dynamics, *Phys. Rept.* **268**, 263 (1996), [arXiv:hep-ph/9505422](#).
- [24] U. Loring, B. C. Metsch, and H. R. Petry, The Light baryon spectrum in a relativistic quark model with instanton induced quark forces: The Nonstrange baryon spectrum and ground states, *Eur. Phys. J. A* **10**, 395 (2001), [arXiv:hep-ph/0103289](#).
- [25] M. M. Giannini, E. Santopinto, and A. Vassallo, Hypercentral constituent quark model and isospin dependence, *Eur. Phys. J. A* **12**, 447 (2001), [arXiv:nucl-th/0111073](#).
- [26] E. Santopinto, An Interacting quark-diquark model of baryons, *Phys. Rev. C* **72**, 022201 (2005), [arXiv:hep-](#)

- ph/0412319.
- [27] R. Bijker, E. Santopinto, and E. Santopinto, Unquenched quark model for baryons: Magnetic moments, spins and orbital angular momenta, *Phys. Rev. C* **80**, 065210 (2009), [arXiv:0912.4494 \[nucl-th\]](#).
- [28] L. Liu, C. Chen, Y. Lu, C. D. Roberts, and J. Segovia, Composition of low-lying $J=3/2$ Δ -baryons, *Phys. Rev. D* **105**, 114047 (2022), [arXiv:2203.12083 \[hep-ph\]](#).
- [29] M. Mai, U.-G. Meißner, and C. Urbach, Towards a theory of hadron resonances, *Phys. Rept.* **1001**, 1 (2023), [arXiv:2206.01477 \[hep-ph\]](#).
- [30] U.-G. Meißner, The Beauty of Spin, *J. Phys. Conf. Ser.* **295**, 012001 (2011), [arXiv:1012.0924 \[hep-ph\]](#).
- [31] C. W. Andersen, J. Bulava, B. Hörz, and C. Morningstar, Elastic $I = 3/2$ p -wave nucleon-pion scattering amplitude and the $\Delta(1232)$ resonance from $N_f=2+1$ lattice QCD, *Phys. Rev. D* **97**, 014506 (2018), [arXiv:1710.01557 \[hep-lat\]](#).
- [32] G. Silvi *et al.*, P -wave nucleon-pion scattering amplitude in the $\Delta(1232)$ channel from lattice QCD, *Phys. Rev. D* **103**, 094508 (2021), [arXiv:2101.00689 \[hep-lat\]](#).
- [33] F. Pittler, C. Alexandrou, K. Hadjiannakou, G. Koutsou, S. Paul, M. Petschlies, and A. Todaro, Elastic $\pi - N$ scattering in the $I = 3/2$ channel, *PoS LATTICE2021*, 226 (2022), [arXiv:2112.04146 \[hep-lat\]](#).
- [34] J. Bulava, A. D. Hanlon, B. Hörz, C. Morningstar, A. Nicholson, F. Romero-López, S. Skinner, P. Vranas, and A. Walker-Loud, Elastic nucleon-pion scattering at $m_\pi=200$ MeV from lattice QCD, *Nucl. Phys. B* **987**, 116105 (2023), [arXiv:2208.03867 \[hep-lat\]](#).
- [35] S. Taylor *et al.* (CLAS), Radiative decays of the $\Sigma_{\Lambda 0}(1385)$ and $\Lambda_{\Lambda}(1520)$ hyperons, *Phys. Rev. C* **71**, 054609 (2005), [Erratum: *Phys.Rev.C* **72**, 039902 (2005)], [arXiv:hep-ex/0503014](#).
- [36] L. S. Geng, E. Oset, and M. Doring, The Radiative decay of the $\Lambda(1405)$ and its two-pole structure, *Eur. Phys. J. A* **32**, 201 (2007), [arXiv:hep-ph/0702093](#).
- [37] M. Döring, Radiative decay of the $\Delta^*(1700)$, *Nucl. Phys. A* **786**, 164 (2007), [arXiv:nucl-th/0701070](#).
- [38] M. Doring, E. Oset, and S. Sarkar, Radiative decay of the $\Lambda(1520)$, *Phys. Rev. C* **74**, 065204 (2006), [arXiv:nucl-th/0601027](#).
- [39] V. I. Mokeev and D. S. Carman (CLAS), Photo- and Electrocouplings of Nucleon Resonances, *Few Body Syst.* **63**, 59 (2022), [arXiv:2202.04180 \[nucl-ex\]](#).
- [40] G. Ramalho and M. T. Peña, Electromagnetic Transition Form Factors of Baryon Resonances, (2023), [arXiv:2306.13900 \[hep-ph\]](#).
- [41] C. E. Carlson and M. Vanderhaeghen, Empirical transverse charge densities in the nucleon and the nucleon-to-Delta transition, *Phys. Rev. Lett.* **100**, 032004 (2008), [arXiv:0710.0835 \[hep-ph\]](#).
- [42] V. Bernard, N. Kaiser, and U.-G. Meißner, On the low-energy theorems for threshold pion electroproduction, *Phys. Lett. B* **282**, 448 (1992).
- [43] V. Bernard, N. Kaiser, T. S. H. Lee, and U.-G. Meißner, Chiral symmetry and threshold $\pi 0$ electroproduction, *Phys. Rev. Lett.* **70**, 387 (1993).
- [44] V. Bernard, N. Kaiser, T. S. H. Lee, and U.-G. Meißner, Threshold pion electroproduction in chiral perturbation theory, *Phys. Rept.* **246**, 315 (1994), [arXiv:hep-ph/9310329](#).
- [45] V. Bernard, N. Kaiser, and U.-G. Meißner, Novel pion electroproduction low-energy theorems, *Phys. Rev. Lett.* **74**, 3752 (1995), [arXiv:hep-ph/9412282](#).
- [46] V. Bernard, N. Kaiser, and U.-G. Meißner, Threshold neutral pion electroproduction in heavy baryon chiral perturbation theory, *Nucl. Phys. A* **607**, 379 (1996), [Erratum: *Nucl.Phys.A* **633**, 695–697 (1998)], [arXiv:hep-ph/9601267](#).
- [47] S. Steininger and U.-G. Meißner, Threshold kaon photo-production and electroproduction in $SU(3)$ baryon chiral perturbation theory, *Phys. Lett. B* **391**, 446 (1997), [arXiv:nucl-th/9609051](#).
- [48] V. Bernard, N. Kaiser, and U.-G. Meißner, The Pion charge radius from charged pion electroproduction, *Phys. Rev. C* **62**, 028201 (2000), [arXiv:nucl-th/0003062](#).
- [49] H. Krebs, V. Bernard, and U.-G. Meißner, Improved analysis of neutral pion electroproduction off deuterium in chiral perturbation theory, *Eur. Phys. J. A* **22**, 503 (2004), [arXiv:nucl-th/0405006](#).
- [50] D. Jido, M. Doering, and E. Oset, Transition form factors of the $N^*(1535)$ as a dynamically generated resonance, *Phys. Rev. C* **77**, 065207 (2008), [arXiv:0712.0038 \[nucl-th\]](#).
- [51] M. Doring, D. Jido, and E. Oset, Helicity Amplitudes of the $\Lambda(1670)$ and two $\Lambda(1405)$ as dynamically generated resonances, *Eur. Phys. J. A* **45**, 319 (2010), [arXiv:1002.3688 \[nucl-th\]](#).
- [52] M. Mai, Review of the $\Lambda(1405)$ A curious case of a strangeness resonance, *Eur. Phys. J. ST* **230**, 1593 (2021), [arXiv:2010.00056 \[nucl-th\]](#).
- [53] T. A. Gail and T. R. Hemmert, Signatures of chiral dynamics in the nucleon to delta transition, *Eur. Phys. J. A* **28**, 91 (2006), [arXiv:nucl-th/0512082](#).
- [54] T. Bauer, S. Scherer, and L. Tiator, Electromagnetic transition form factors of the Roper resonance in effective field theory, *Phys. Rev. C* **90**, 015201 (2014), [arXiv:1402.0741 \[nucl-th\]](#).
- [55] D. Merten, U. Loring, K. Kretzschmar, B. Metsch, and H. R. Petry, Electroweak form-factors of nonstrange baryons, *Eur. Phys. J. A* **14**, 477 (2002), [arXiv:hep-ph/0204024](#).
- [56] F. Gross, G. Ramalho, and M. T. Pena, A Pure S-wave covariant model for the nucleon, *Phys. Rev. C* **77**, 015202 (2008), [arXiv:nucl-th/0606029](#).
- [57] G. Ramalho and M. T. Pena, A covariant model for the $\gamma N \rightarrow N(1535)$ transition at high momentum transfer, *Phys. Rev. D* **84**, 033007 (2011), [arXiv:1105.2223 \[hep-ph\]](#).
- [58] E. Santopinto and M. M. Giannini, Systematic study of longitudinal and transverse helicity amplitudes in the hypercentral constituent quark model, *Phys. Rev. C* **86**, 065202 (2012), [arXiv:1506.01207 \[nucl-th\]](#).
- [59] B. Golli and S. Širca, A chiral quark model for meson electroproduction in the region of D-wave resonances, *Eur. Phys. J. A* **49**, 111 (2013), [arXiv:1306.3330 \[nucl-th\]](#).
- [60] I. G. Aznauryan and V. Burkert, Electroexcitation of nucleon resonances of the $[70,1-]$ multiplet in a light-front relativistic quark model, *Phys. Rev. C* **95**, 065207 (2017), [arXiv:1703.01751 \[nucl-th\]](#).
- [61] I. T. Obukhovskiy, A. Faessler, D. K. Fedorov, T. Gutsche, and V. E. Lyubovitskij, Transition form factors and helicity amplitudes for electroexcitation of negative- and positive parity nucleon resonances in a light-front quark model, *Phys. Rev. D* **100**, 094013 (2019), [arXiv:1909.13787 \[hep-ph\]](#).

- [62] G. Ramalho and M. T. Peña, Covariant model for the Dalitz decay of the $N(1535)$ resonance, *Phys. Rev. D* **101**, 114008 (2020), arXiv:2003.04850 [hep-ph].
- [63] B. Borasoy, P. C. Bruns, U.-G. Meißner, and R. Nissler, A Gauge invariant chiral unitary framework for kaon photo- and electroproduction on the proton, *Eur. Phys. J. A* **34**, 161 (2007), arXiv:0709.3181 [nucl-th].
- [64] D. Ruić, M. Mai, and U.-G. Meißner, η -Photoproduction in a gauge-invariant chiral unitary framework, *Phys. Lett. B* **704**, 659 (2011), arXiv:1108.4825 [nucl-th].
- [65] M. Mai, P. C. Bruns, and U.-G. Meißner, Pion photoproduction off the proton in a gauge-invariant chiral unitary framework, *Phys. Rev. D* **86**, 094033 (2012), arXiv:1207.4923 [nucl-th].
- [66] I. C. Cloet, G. Eichmann, B. El-Bennich, T. Klahn, and C. D. Roberts, Survey of nucleon electromagnetic form factors, *Few Body Syst.* **46**, 1 (2009), arXiv:0812.0416 [nucl-th].
- [67] D. J. Wilson, I. C. Cloet, L. Chang, and C. D. Roberts, Nucleon and Roper electromagnetic elastic and transition form factors, *Phys. Rev. C* **85**, 025205 (2012), arXiv:1112.2212 [nucl-th].
- [68] J. Segovia, B. El-Bennich, E. Rojas, I. C. Cloet, C. D. Roberts, S.-S. Xu, and H.-S. Zong, Completing the picture of the Roper resonance, *Phys. Rev. Lett.* **115**, 171801 (2015), arXiv:1504.04386 [nucl-th].
- [69] G. Eichmann, C. S. Fischer, and H. Sanchis-Alepuz, Light baryons and their excitations, *Phys. Rev. D* **94**, 094033 (2016), arXiv:1607.05748 [hep-ph].
- [70] C. Chen, Y. Lu, D. Binosi, C. D. Roberts, J. Rodríguez-Quintero, and J. Segovia, Nucleon-to-Roper electromagnetic transition form factors at large Q^2 , *Phys. Rev. D* **99**, 034013 (2019), arXiv:1811.08440 [nucl-th].
- [71] S.-X. Qin, C. D. Roberts, and S. M. Schmidt, Spectrum of light- and heavy-baryons, *Few Body Syst.* **60**, 26 (2019), arXiv:1902.00026 [nucl-th].
- [72] I. G. Aznauryan and V. D. Burkert, Electroexcitation of nucleon resonances, *Prog. Part. Nucl. Phys.* **67**, 1 (2012), arXiv:1109.1720 [hep-ph].
- [73] I. G. Aznauryan *et al.*, Studies of Nucleon Resonance Structure in Exclusive Meson Electroproduction, *Int. J. Mod. Phys. E* **22**, 1330015 (2013), arXiv:1212.4891 [nucl-th].
- [74] A. Bashir, L. Chang, I. C. Cloet, B. El-Bennich, Y.-X. Liu, C. D. Roberts, and P. C. Tandy, Collective perspective on advances in Dyson-Schwinger Equation QCD, *Commun. Theor. Phys.* **58**, 79 (2012), arXiv:1201.3366 [nucl-th].
- [75] G. Eichmann, H. Sanchis-Alepuz, R. Williams, R. Alkofer, and C. S. Fischer, Baryons as relativistic three-quark bound states, *Prog. Part. Nucl. Phys.* **91**, 1 (2016), arXiv:1606.09602 [hep-ph].
- [76] G. Eichmann, Theory Introduction to Baryon Spectroscopy, *Few Body Syst.* **63**, 57 (2022), arXiv:2202.13378 [hep-ph].
- [77] A. Agadjanov, V. Bernard, U. G. Meißner, and A. Rusetsky, A framework for the calculation of the $\Delta N \gamma^*$ transition form factors on the lattice, *Nucl. Phys. B* **886**, 1199 (2014), arXiv:1405.3476 [hep-lat].
- [78] A. Radhakrishnan, J. J. Dudek, and R. G. Edwards (Hadron Spectrum), Radiative decay of the resonant K^* and the $\gamma K \rightarrow K \pi$ amplitude from lattice QCD, *Phys. Rev. D* **106**, 114513 (2022), arXiv:2208.13755 [hep-lat].
- [79] L. Tiator, M. Döring, R. L. Workman, M. Hadžimehmedović, H. Osmanović, R. Omerović, J. Stahov, and A. Švarc, Baryon transition form factors at the pole, *Phys. Rev. C* **94**, 065204 (2016), arXiv:1606.00371 [nucl-th].
- [80] L. Tiator, R. L. Workman, Y. Wunderlich, and H. Haberzettl, Amplitude reconstruction from complete electroproduction experiments and truncated partial-wave expansions, *Phys. Rev. C* **96**, 025210 (2017), arXiv:1702.08375 [nucl-th].
- [81] Y. Wunderlich, New graphical criterion for the selection of complete sets of polarization observables and its application to single-meson photoproduction as well as electroproduction, *Phys. Rev. C* **104**, 045203 (2021), arXiv:2106.00486 [nucl-th].
- [82] M. Mai, M. Döring, C. Granados, H. Haberzettl, U.-G. Meißner, D. Rönchen, I. Strakovsky, and R. Workman (Jülich-Bonn-Washington), Jülich-Bonn-Washington model for pion electroproduction multipoles, *Phys. Rev. C* **103**, 065204 (2021), arXiv:2104.07312 [nucl-th].
- [83] M. Mai, M. Döring, C. Granados, H. Haberzettl, J. Hergenrath, U.-G. Meißner, D. Rönchen, I. Strakovsky, and R. Workman (Jülich-Bonn-Washington), Coupled-channels analysis of pion and η electroproduction within the Jülich-Bonn-Washington model, *Phys. Rev. C* **106**, 015201 (2022), arXiv:2111.04774 [nucl-th].
- [84] D. Rönchen, M. Döring, H. Haberzettl, J. Haidenbauer, U.-G. Meißner, and K. Nakayama, Eta photoproduction in a combined analysis of pion- and photon-induced reactions, *Eur. Phys. J. A* **51**, 70 (2015), arXiv:1504.01643 [nucl-th].
- [85] D. Rönchen, M. Döring, and U.-G. Meißner, The impact of $K^+ \Lambda$ photoproduction on the resonance spectrum, *Eur. Phys. J. A* **54**, 110 (2018), arXiv:1801.10458 [nucl-th].
- [86] D. Rönchen, M. Döring, U.-G. Meißner, and C.-W. Shen, Light baryon resonances from a coupled-channel study including $K \Sigma$ photoproduction, *Eur. Phys. J. A* **58**, 229 (2022), arXiv:2208.00089 [nucl-th].
- [87] Y.-F. Wang, D. Rönchen, U.-G. Meißner, Y. Lu, C.-W. Shen, and J.-J. Wu, Reaction $\pi N \rightarrow \omega N$ in a dynamical coupled-channel approach, *Phys. Rev. D* **106**, 094031 (2022), arXiv:2208.03061 [nucl-th].
- [88] M. Döring, C. Hanhart, F. Huang, S. Krewald, U.-G. Meißner, and D. Rönchen, The reaction $\pi^+ p \rightarrow K^+ \Sigma^+$ in a unitary coupled-channels model, *Nucl. Phys. A* **851**, 58 (2011), arXiv:1009.3781 [nucl-th].
- [89] D. Ronchen, M. Doring, F. Huang, H. Haberzettl, J. Haidenbauer, C. Hanhart, S. Krewald, U.-G. Meißner, and K. Nakayama, Coupled-channel dynamics in the reactions $\pi N \rightarrow \pi N$, ηN , $K \Lambda$, $K \Sigma$, *Eur. Phys. J. A* **49**, 44 (2013), arXiv:1211.6998 [nucl-th].
- [90] Jülich-Bonn web page with fit results for pion and photon-induced reactions, http://collaborations.fz-juelich.de/ikp/meson-baryon/juelich_amplitudes.html (2012).
- [91] JBW Interactive Scattering Analysis website (under development), <https://JBW.phys.gwu.edu> (2021).
- [92] L. Tiator, D. Drechsel, S. Kamalov, M. M. Giannini, E. Santopinto, and A. Vassallo, Electroproduction of nucleon resonances, *Eur. Phys. J. A* **19**, 55 (2004), arXiv:nucl-th/0310041.
- [93] M. Hilt, B. C. Lehnhart, S. Scherer, and L. Tiator, Pion photo- and electroproduction in relativistic baryon chi-

- ral perturbation theory and the chiral MAID interface, *Phys. Rev. C* **88**, 055207 (2013), [arXiv:1309.3385 \[nucl-th\]](#).
- [94] W.-T. Chiang, S.-N. Yang, L. Tiator, and D. Drechsel, An Isobar model for eta photoproduction and electroproduction on the nucleon, *Nucl. Phys. A* **700**, 429 (2002), [arXiv:nucl-th/0110034](#).
- [95] L. Tiator, D. Drechsel, S. S. Kamalov, and M. Vanderhaeghen, Electromagnetic Excitation of Nucleon Resonances, *Eur. Phys. J. ST* **198**, 141 (2011), [arXiv:1109.6745 \[nucl-th\]](#).
- [96] I. G. Aznauryan *et al.* (CLAS), Electroexcitation of nucleon resonances from CLAS data on single pion electroproduction, *Phys. Rev. C* **80**, 055203 (2009), [arXiv:0909.2349 \[nucl-ex\]](#).
- [97] V. D. Burkert and C. D. Roberts, Colloquium : Roper resonance: Toward a solution to the fifty year puzzle, *Rev. Mod. Phys.* **91**, 011003 (2019), [arXiv:1710.02549 \[nucl-ex\]](#).
- [98] V. D. Burkert, Nucleon resonances and transition form factors, (2022), [arXiv:2212.08980 \[hep-ph\]](#).
- [99] I. G. Aznauryan, Multipole amplitudes of pion photoproduction on nucleons up to 2-GeV within dispersion relations and unitary isobar model, *Phys. Rev. C* **67**, 015209 (2003), [arXiv:nucl-th/0206033](#).
- [100] I. G. Aznauryan *et al.* (CLAS), Electroexcitation of the Roper resonance for $1.7 < Q^{*2} < 4.5$ -GeV² in $\text{vec-ep} \rightarrow \text{en pi}^+$, *Phys. Rev. C* **78**, 045209 (2008), [arXiv:0804.0447 \[nucl-ex\]](#).
- [101] S. X. Nakamura, H. Kamano, and T. Sato, Dynamical coupled-channels model for neutrino-induced meson productions in resonance region, *Phys. Rev. D* **92**, 074024 (2015), [arXiv:1506.03403 \[hep-ph\]](#).
- [102] G. Ramalho, Analytic parametrizations of the $\gamma^* N \rightarrow N(1440)$ form factors inspired by light-front holography, *Phys. Rev. D* **96**, 054021 (2017), [arXiv:1706.05707 \[hep-ph\]](#).
- [103] G. Ramalho, Combined parametrization of G_{En} and $\gamma^* N \rightarrow \Delta(1232)$ quadrupole form factors, *Eur. Phys. J. A* **55**, 32 (2019), [arXiv:1710.10527 \[hep-ph\]](#).
- [104] G. Ramalho, Low- Q^2 empirical parametrizations of the N^* helicity amplitudes, *Phys. Rev. D* **100**, 114014 (2019), [arXiv:1909.00013 \[hep-ph\]](#).
- [105] V. I. Mokeev *et al.* (CLAS), Experimental Study of the $P_{11}(1440)$ and $D_{13}(1520)$ resonances from CLAS data on $ep \rightarrow e'\pi^+\pi^-p'$, *Phys. Rev. C* **86**, 035203 (2012), [arXiv:1205.3948 \[nucl-ex\]](#).
- [106] V. I. Mokeev *et al.*, New Results from the Studies of the $N(1440)1/2^+$, $N(1520)3/2^-$, and $\Delta(1620)1/2^-$ Resonances in Exclusive $ep \rightarrow e'p'\pi^+\pi^-$ Electroproduction with the CLAS Detector, *Phys. Rev. C* **93**, 025206 (2016), [arXiv:1509.05460 \[nucl-ex\]](#).
- [107] V. I. Mokeev *et al.*, Evidence for the $N'(1720)3/2^+$ Nucleon Resonance from Combined Studies of CLAS $\pi^+\pi^-p$ Photo- and Electroproduction Data, *Phys. Lett. B* **805**, 135457 (2020), [arXiv:2004.13531 \[nucl-ex\]](#).
- [108] V. I. Mokeev, P. Achenbach, V. D. Burkert, D. S. Carman, R. W. Gothe, A. N. Hiller Blin, E. L. Isupov, K. Joo, K. Neupane, and A. Trivedi, First Results on Nucleon Resonance Electroexcitation Amplitudes from $ep \rightarrow e'\pi^+\pi^-p'$ Cross Sections at W from 1.4-1.7 GeV and Q^2 from 2.0-5.0 GeV², (2023), [arXiv:2306.13777 \[nucl-ex\]](#).
- [109] V. Bernard, N. Kaiser, U. G. Meißner, and A. Schmidt, Threshold two pion photoproduction and electroproduction: More neutrals than expected, *Nucl. Phys. A* **580**, 475 (1994), [arXiv:nucl-th/9403013](#).
- [110] C. Bennhold, H. Haberzettl, and T. Mart, A New resonance in K^+ Lambda electroproduction: The $D(13)(1895)$ and its electromagnetic form-factors, in *2nd ICTP International Conference on Perspectives in Hadronic Physics* (1999) pp. 328–337, [arXiv:nucl-th/9909022](#).
- [111] O. V. Maxwell, Electromagnetic production of kaons from protons, and baryon electromagnetic form factors, *Phys. Rev. C* **85**, 034611 (2012).
- [112] T. Corthals, T. Van Cauteren, P. Van Craeyveld, J. Ryckebusch, and D. G. Ireland, Electroproduction of kaons from the proton in a Regge-plus-resonance approach, *Phys. Lett. B* **656**, 186 (2007), [arXiv:0704.3691 \[nucl-th\]](#).
- [113] L. De Cruz, J. Ryckebusch, T. Vrancx, and P. Van Craeyveld, A Bayesian analysis of kaon photoproduction with the Regge-plus-resonance model, *Phys. Rev. C* **86**, 015212 (2012), [arXiv:1205.2195 \[nucl-th\]](#).
- [114] D. S. Carman, CLAS \bar{N}^* Excitation Results from Pion and Kaon Electroproduction, *Few Body Syst.* **59**, 82 (2018).
- [115] H. Haberzettl, C. Bennhold, T. Mart, and T. Feuster, Gauge-invariant tree-level photoproduction amplitudes with form factors, *Phys. Rev. C* **58**, R40 (1998), [arXiv:nucl-th/9804051](#).
- [116] T. Mart and C. Bennhold, Evidence for a missing nucleon resonance in kaon photoproduction, *Phys. Rev. C* **61**, 012201 (2000), [arXiv:nucl-th/9906096](#).
- [117] T. Mart and A. Sulaksono, Kaon photoproduction in a multipole approach, *Phys. Rev. C* **74**, 055203 (2006), [arXiv:nucl-th/0609077](#).
- [118] T. Mart, Photo- and electroproduction of the $K^0\Lambda$ near threshold and effects of the K^0 electromagnetic form factor, *Phys. Rev. C* **83**, 048203 (2011), [arXiv:1104.2393 \[nucl-th\]](#).
- [119] J. Nys, V. Mathieu, C. Fernández-Ramírez, A. N. Hiller Blin, A. Jackura, M. Mikhasenko, A. Pilloni, A. P. Szczepaniak, G. Fox, and J. Ryckebusch (JPAC), Finite-energy sum rules in eta photoproduction off a nucleon, *Phys. Rev. D* **95**, 034014 (2017), [arXiv:1611.04658 \[hep-ph\]](#).
- [120] A. N. H. Blin, W. Melnitchouk, V. I. Mokeev, V. D. Burkert, V. V. Chesnokov, A. Pilloni, and A. P. Szczepaniak, Resonant contributions to inclusive nucleon structure functions from exclusive meson electroproduction data, *Phys. Rev. C* **104**, 025201 (2021), [arXiv:2105.05834 \[hep-ph\]](#).
- [121] H. Haberzettl, Gauge invariance of meson photo- and electroproduction currents revisited, *Phys. Rev. D* **104**, 056001 (2021), [arXiv:2105.11554 \[hep-ph\]](#).
- [122] D. S. Carman *et al.* (CLAS), Beam-recoil transferred polarization in $K+Y$ electroproduction in the nucleon resonance region with CLAS12, *Phys. Rev. C* **105**, 065201 (2022), [arXiv:2202.03398 \[nucl-ex\]](#).
- [123] G. F. Chew, M. L. Goldberger, F. E. Low, and Y. Nambu, Relativistic dispersion relation approach to photomeson production, *Phys. Rev.* **106**, 1345 (1957).
- [124] P. Dennery, Theory of the Electro- and Photoproduction of pi Mesons, *Phys. Rev.* **124**, 2000 (1961).
- [125] F. A. Berends, A. Donnachie, and D. L. Weaver, Photo-

- production and electroproduction of pions. 1. Dispersion relation theory, *Nucl. Phys. B* **4**, 1 (1967).
- [126] C. Ciofi Degli Atti, ELECTRON SCATTERING BY NUCLEI, *Prog. Part. Nucl. Phys.* **3**, 163 (1978).
- [127] M. Doring, C. Hanhart, F. Huang, S. Krewald, and U.-G. Meißner, Analytic properties of the scattering amplitude and resonances parameters in a meson exchange model, *Nucl. Phys. A* **829**, 170 (2009), [arXiv:0903.4337 \[nucl-th\]](#).
- [128] M. Doring, C. Hanhart, F. Huang, S. Krewald, and U.-G. Meißner, The Role of the background in the extraction of resonance contributions from meson-baryon scattering, *Phys. Lett. B* **681**, 26 (2009), [arXiv:0903.1781 \[nucl-th\]](#).
- [129] A. J. F. Siegert, Note on the interaction between nuclei and electromagnetic radiation, *Phys. Rev.* **52**, 787 (1937).
- [130] L. Tiator, Pion Electroproduction and Siegert's Theorem, *Few Body Syst.* **57**, 1087 (2016).
- [131] C. Mertz *et al.*, Search for quadrupole strength in the electroexcitation of the delta(1232), *Phys. Rev. Lett.* **86**, 2963 (2001), [arXiv:nucl-ex/9902012](#).
- [132] D. Elsner *et al.*, Measurement of the LT-asymmetry in pi0 electroproduction at the energy of the Delta(1232) resonance, *Eur. Phys. J. A* **27**, 91 (2006), [arXiv:nucl-ex/0507014](#).
- [133] K. Joo *et al.* (CLAS), Measurement of the polarized structure function sigma(LT-prime) for p(polarized-p, e-prime p) pi0 in the Delta(1232) resonance region, *Phys. Rev. C* **68**, 032201 (2003), [arXiv:nucl-ex/0301012](#).
- [134] N. F. Sparveris *et al.* (OOPS), Measurement of the R(LT) response function for pi0 electroproduction at Q**2 = 0.070 (GeV/c)**2 in the N -> Delta transition, *Phys. Rev. C* **67**, 058201 (2003), [arXiv:nucl-ex/0212022](#).
- [135] J. J. Kelly *et al.* (Jefferson Lab Hall A), Recoil polarization for delta excitation in pion electroproduction, *Phys. Rev. Lett.* **95**, 102001 (2005), [arXiv:nucl-ex/0505024](#).
- [136] P. Bartsch *et al.*, Measurement of the beam helicity asymmetry in the p(polarized-e, e-prime p) pi0 reaction at the energy of the Delta(1232) resonance, *Phys. Rev. Lett.* **88**, 142001 (2002), [arXiv:nucl-ex/0112009](#).
- [137] I. K. Bensafa *et al.* (MAMI-A1), Beam-helicity asymmetry in photon and pion electroproduction in the Delta(1232) resonance region at Q**2 = 0.35 (GeV/c)**2, *Eur. Phys. J. A* **32**, 69 (2007), [arXiv:hep-ph/0612248](#).
- [138] K. Joo *et al.* (CLAS), Measurement of the polarized structure function sigma(LT-prime) for p(polarized-e, e-prime pi+)n in the Delta(1232) resonance region, *Phys. Rev. C* **70**, 042201 (2004), [arXiv:nucl-ex/0407013](#).
- [139] K. Park, private communication, (2007).
- [140] D. Gaskell *et al.*, Longitudinal electroproduction of charged pions from H-1, H-2, He-3, *Phys. Rev. Lett.* **87**, 202301 (2001).
- [141] G. Laveissiere *et al.* (JLab Hall A), Backward electroproduction of pi0 mesons on protons in the region of nucleon resonances at four momentum transfer squared Q**2 = 1.0-GeV**2, *Phys. Rev. C* **69**, 045203 (2004), [arXiv:nucl-ex/0308009](#).
- [142] M. Ungaro *et al.* (CLAS), Measurement of the N -> Delta+(1232) transition at high momentum transfer by pi0 electroproduction, *Phys. Rev. Lett.* **97**, 112003 (2006), [arXiv:hep-ex/0606042](#).
- [143] J. Gayler, *Electroproduction of pi0 mesons in the region of Delta(1232) with momentum transfer q^2 = 15 fm^-2*, Tech. Rep. DESY-F21-71-2 (DESY, 1971).
- [144] J. May, *Koinzidenzmessungen zur Untersuchung der Reaktion ep -> ep pi0 beim Impulsübertrag q^2 approx 1 GeV^2 im Massenbereich zwischen 1.136 und 1.316 GeV*, Ph.D. thesis, Hamburg U. (1971).
- [145] V. V. Frolov *et al.*, Electroproduction of the Delta (1232) resonance at high momentum transfer, *Phys. Rev. Lett.* **82**, 45 (1999), [arXiv:hep-ex/9808024](#).
- [146] C. T. Hill, *Higgs Scalars and the Nonleptonic Weak Interactions*, Other thesis, Caltech (1977).
- [147] K. Joo *et al.* (CLAS), Q**2 dependence of quadrupole strength in the gamma* p -> Delta+(1232) -> p pi0 transition, *Phys. Rev. Lett.* **88**, 122001 (2002), [arXiv:hep-ex/0110007](#).
- [148] R. Siddle *et al.*, Coincidence pi0 electroproduction experiments in the first resonance region at momentum transfers of 0.3, 0.45, 0.60, 0.76 GeV/c^2, *Nucl. Phys. B* **35**, 93 (1971).
- [149] R. Haidan, *Elektroproduktion pseudoskalarer Mesonen im Resonanzgebiet bei großen Impulsüberträgen*, Ph.D. thesis, Hamburg U. (1979).
- [150] F. Kalleicher, U. Dittmayer, R. W. Gothe, H. Putsch, T. Reichelt, B. Schoch, and M. Wilhelm, The determination of sigma(LT)/sigma(TT) in electro pion production in the Delta resonance region, *Z. Phys. A* **359**, 201 (1997).
- [151] K. Baetzner *et al.*, Pi0 electroproduction at the delta(1236) resonance at a four-momentum transfer of q-squared = 0.3(gev/c)-squared, *Nucl. Phys. B* **76**, 1 (1974).
- [152] A. Latham *et al.*, Coincidence electroproduction of single neutral pions in the resonance region at q^2 = 0.5 (GeV/c)^2, *Nucl. Phys. B* **156**, 58 (1979).
- [153] A. Latham *et al.*, Electroproduction of pi0 Mesons in the Resonance Region at q^2 = 1.0-{GeV}/c^2, *Nucl. Phys. B* **189**, 1 (1981).
- [154] S. C. Stave, *Lowest Q^2 Measurement of the gamma*p -> Delta Reaction: Probing the Pionic Contribution*, Ph.D. thesis, MIT (2006).
- [155] N. F. Sparveris *et al.*, Determination of quadrupole strengths in the gamma* p -> Delta(1232) transition at Q**2 = 0.20-(GeV/c)**2, *Phys. Lett. B* **651**, 102 (2007), [arXiv:nucl-ex/0611033](#).
- [156] J. C. Alder, F. W. Brasse, W. Fehrenbach, J. Gayler, S. P. Goel, R. Haidan, V. Korbel, J. May, M. Merkwitz, and A. Nurimba, Electroproduction of neutral pions in the resonance region, *Nucl. Phys. B* **105**, 253 (1976).
- [157] N. G. Afanasev, A. S. Esaulov, A. M. Pilipenko, and Y. I. Titov, Separation of Transversal and Longitudinal Components of Cross-Section of Pion Electroproduction on Proton Near the Threshold, *Pisma Zh. Eksp. Teor. Fiz.* **22**, 400 (1975).
- [158] W. J. Shuttleworth *et al.*, Coincidence pi0 electroproduction in the second resonance region, *Nucl. Phys. B* **45**, 428 (1972).
- [159] H. Blume, R. Farber, N. Feldmann, K. Heinloth, D. Kramarczyk, F. Kuckelkorn, H. J. Michels, J. Pasler, and J. P. Dowd, ELECTROPRODUCTION OF pi0 MESONS ON PROTONS AT W = 1400-MeV TO 2000-MeV, q**2 = 0.01-GeV**2 TO 0.1-GeV**2, AND t = 0.6-GeV**2 TO 2.2-GeV**2 CORRESPONDING TO Theta (CM) pi = 145-degrees TO 180-degrees, *Z. Phys.*

- C **16**, 283 (1983).
- [160] M. Rosenberg, *Electroproduction of Neutral π Mesons in the Range of the Two Nucleon Resonance at 0.3 GeV²/c² Momentum Transfer*, Thesis, Bonn (1979).
- [161] V. Gerhardt, *Pion-Elektroproduktion im Bereich der 2. und 3. Nukleonresonanz*, Ph.D. thesis, Hamburg U. (1979).
- [162] MONTANA, "Pion electroproduction $\pi^0 p$ ", Ph.D. thesis, Harvard (1971).
- [163] H. Egiyan *et al.* (CLAS), Single π^+ electroproduction on the proton in the first and second resonance regions at $0.25\text{-GeV}^2 < Q^2 < 0.65\text{-GeV}^2$ using CLAS, *Phys. Rev. C* **73**, 025204 (2006), [arXiv:nucl-ex/0601007](#).
- [164] H. Breuker *et al.*, Forward π^+ Electroproduction in the First Resonance Region at Four Momentum Transfers $q^2 = 0.15\text{-}(GeV/c)^2$ and $0.3\text{-}(GeV/c)^2$, *Nucl. Phys. B* **146**, 285 (1978).
- [165] G. Bardin, J. Duclos, J. Julien, A. Magnon, B. Michel, and J. C. Montret, A measurement of the longitudinal and transverse parts of the π^+ electroproduction cross-section at 1175 MeV pion-nucleon centre-of-mass energy., *Lett. Nuovo Cim.* **13**, 485 (1975).
- [166] G. Bardin, J. Duclos, A. Magnon, B. Michel, and J. C. Montret, A Transverse and Longitudinal Cross-Section Separation in a π^+ Electroproduction Coincidence Experiment and the Pion Radius, *Nucl. Phys. B* **120**, 45 (1977).
- [167] M. Davenport, *Electroproduction of neutral and positive pions between the first and second resonance regions.*, Ph.D. thesis, Lancaster (1980).
- [168] O. Vapenikova *et al.*, Electroproduction of Single Charged Pions from Deuterium at $Q^2 \approx 1\text{ GeV}^2$ in the Resonance Region, *Z. Phys. C* **37**, 251 (1988).
- [169] J. C. Alder, H. Behrens, F. W. Brasse, W. Fehrenbach, J. Gayler, S. P. Goel, R. Haidan, V. Korbel, J. May, and M. Merkwitz, Electroproduction of π^+ Mesons in the Resonance Region, *Nucl. Phys. B* **99**, 1 (1975).
- [170] E. Evangelides *et al.*, Electroproduction of π^+ mesons in the second and third resonance regions, *Nucl. Phys. B* **71**, 381 (1974).
- [171] H. Breuker *et al.*, Electroproduction of π^+ Mesons at Forward and Backward Direction in the Region of the D^{-13} (1520) and ^{15}F (1688) Resonances, *Z. Phys. C* **13**, 113 (1982).
- [172] H. Breuker *et al.*, Backward Electroproduction of π^+ Mesons in the Second and Third Nucleon Resonance Region, *Z. Phys. C* **17**, 121 (1983).
- [173] C. J. Bebek, C. N. Brown, M. Herzlinger, S. D. Holmes, C. A. Lichtenstein, F. M. Pipkin, S. Raither, and L. K. Sistierson, Measurement of the pion form-factor up to $q^2 = 4\text{-GeV}^2$, *Phys. Rev. D* **13**, 25 (1976).
- [174] C. N. Brown, C. R. Canizares, W. E. Cooper, A. M. Eisner, G. J. Feldmann, C. A. Lichtenstein, L. Litt, W. Loceretz, V. B. Montana, and F. M. Pipkin, Coincidence electroproduction of charged pions and the pion form-factor, *Phys. Rev. D* **8**, 92 (1973).
- [175] L. Litt, *PI+ ELECTROPRODUCTION ALONG THE VIRTUAL PHOTON AT FIXED k^2* , Other thesis, unknown (1971).
- [176] C. S. Armstrong *et al.* (Jefferson Lab E94014), Electroproduction of the S(11)(1535) resonance at high momentum transfer, *Phys. Rev. D* **60**, 052004 (1999), [arXiv:nucl-ex/9811001](#).
- [177] H. Denizli *et al.* (CLAS), Q^2 dependence of the S(11)(1535) photocoupling and evidence for a P-wave resonance in eta electroproduction, *Phys. Rev. C* **76**, 015204 (2007), [arXiv:0704.2546 \[nucl-ex\]](#).
- [178] R. Thompson *et al.* (CLAS), The $e p \rightarrow e' p$ eta reaction at and above the S(11)(1535) baryon resonance, *Phys. Rev. Lett.* **86**, 1702 (2001), [arXiv:hep-ex/0011029](#).
- [179] M. M. Dalton *et al.*, Electroproduction of Eta Mesons in the S(11)(1535) Resonance Region at High Momentum Transfer, *Phys. Rev. C* **80**, 015205 (2009), [arXiv:0804.3509 \[hep-ex\]](#).
- [180] D. S. Carman, K. Park, B. A. Raue, and V. Crede (CLAS), Separated Structure Functions for Exclusive $K^+\Lambda$ and $K^+\Sigma^0$ Electroproduction at 5.5 GeV with CLAS, *Phys. Rev. C* **87**, 025204 (2013), [arXiv:1212.1336 \[nucl-ex\]](#).
- [181] P. Ambrozewicz *et al.* (CLAS), Separated structure functions for the exclusive electroproduction of $K^+\Lambda$ and $K^+\Sigma^0$ final states, *Phys. Rev. C* **75**, 045203 (2007), [arXiv:hep-ex/0611036](#).
- [182] C. Kunz *et al.* (MIT-Bates OOPS), Measurement of the transverse longitudinal cross-sections in the p (polarized-e, e-prime p) π^0 reaction in the Delta region, *Phys. Lett. B* **564**, 21 (2003), [arXiv:nucl-ex/0302018](#).
- [183] S. Stave *et al.*, Lowest Q^2 Measurement of the $\gamma^* p \rightarrow \Delta$ Reaction: Probing the Pionic Contribution, *Eur. Phys. J. A* **30**, 471 (2006), [arXiv:nucl-ex/0604013](#).
- [184] N. F. Sparveris *et al.* (OOPS), Investigation of the conjectured nucleon deformation at low momentum transfer, *Phys. Rev. Lett.* **94**, 022003 (2005), [arXiv:nucl-ex/0408003](#).
- [185] R. Nasseripour *et al.* (CLAS), Polarized Structure Function sigma(LT-prime) for p(polarized-e, e-prime K^+) Lambda in the Nucleon Resonance Region, *Phys. Rev. C* **77**, 065208 (2008), [arXiv:0801.4711 \[nucl-ex\]](#).
- [186] G. A. Warren *et al.* (M.I.T.-Bates OOPS, FPP), Induced proton polarization for π^0 electroproduction at $Q^2 = 0.126\text{ GeV}^2/c^2$ around the Delta (1232) resonance, *Phys. Rev. C* **58**, 3722 (1998), [arXiv:nucl-ex/9901004](#).
- [187] T. Pospischil *et al.*, Measurement of the recoil polarization in the p (polarized e, e-prime polarized p) π^0 reaction at the Delta(1232) resonance, *Phys. Rev. Lett.* **86**, 2959 (2001), [arXiv:nucl-ex/0010020](#).
- [188] J. Blatt and V. Weisskopf, *Theoretical Nuclear Physics* (John Wiley & Sons, New York, 1952).
- [189] D. M. Manley, R. A. Arndt, Y. Goradia, and V. L. Teplitz, An Isobar Model Partial Wave Analysis of $\pi N \rightarrow \pi\pi N$ in the Center-of-mass Energy Range 1320-MeV to 1930-MeV, *Phys. Rev. D* **30**, 904 (1984).
- [190] "Pegasus" cluster at the GW High-Performance Computing facility, <https://hpc.gwu.edu/pegasus/>.
- [191] J. Müller *et al.* (CBELSA/TAPS), New data on $\vec{\gamma} p \rightarrow \eta p$ with polarized photons and protons and their implications for $N^* \rightarrow N\eta$ decays, *Phys. Lett. B* **803**, 135323 (2020), [arXiv:1909.08464 \[nucl-ex\]](#).
- [192] F. X. Lee, T. Mart, C. Bennhold, and L. E. Wright, Quasifree kaon photoproduction on nuclei, *Nucl. Phys. A* **695**, 237 (2001), [arXiv:nucl-th/9907119](#).
- [193] J.-X. Lu, L.-S. Geng, M. Doering, and M. Mai, Cross-Channel Constraints on Resonant Antikaon-Nucleon Scattering, *Phys. Rev. Lett.* **130**, 071902 (2023), [arXiv:2209.02471 \[hep-ph\]](#).
- [194] A. V. Anisovich *et al.*, The impact of new polarization data from Bonn, Mainz and Jefferson Laboratory on

- $\gamma p \rightarrow \pi N$ multipoles, *Eur. Phys. J. A* **52**, 284 (2016), [arXiv:1604.05704 \[nucl-th\]](#).
- [195] W. J. Briscoe, M. Döring, H. Haberzettl, D. M. Manley, M. Naruki, I. I. Strakovsky, and E. S. Swanson, Physics opportunities with meson beams, *Eur. Phys. J. A* **51**, 129 (2015), [arXiv:1503.07763 \[hep-ph\]](#).
- [196] W. J. Briscoe, M. Döring, H. Haberzettl, D. M. Manley, M. Naruki, G. Smith, I. Strakovsky, and E. S. Swanson, Physics Opportunities with Meson Beams for EIC, (2021), [arXiv:2108.07591 \[nucl-ex\]](#).
- [197] D. S. Carman *et al.* (CLAS), First measurement of transferred polarization in the exclusive $\bar{e}p \rightarrow e'K^+\Lambda$ reaction, *Phys. Rev. Lett.* **90**, 131804 (2003), [arXiv:hep-ex/0212014](#).
- [198] D. S. Carman *et al.* (CLAS), Beam-Recoil Polarization Transfer in the Nucleon Resonance Region in the Exclusive $\text{vec-ep} \rightarrow \text{e-prime K+ vec-Lambda}$ and $\text{vec-ep} \rightarrow \text{e-prime K+ vec-Sigma0}$ Reactions at CLAS, *Phys. Rev. C* **79**, 065205 (2009), [arXiv:0904.3246 \[hep-ex\]](#).
- [199] R. K. Bradford *et al.* (CLAS), First measurement of beam-recoil observables $C(x)$ and $C(z)$ in hyperon photoproduction, *Phys. Rev. C* **75**, 035205 (2007), [arXiv:nucl-ex/0611034](#).
- [200] B. A. Raue and D. S. Carman, Ratio of $\sigma(L) / \sigma(T)$ for $p(e, e'\text{-prime K+})\Lambda$ extracted from polarization transfer, *Phys. Rev. C* **71**, 065209 (2005), [arXiv:nucl-ex/0402024](#).
- [201] R. M. Møhring *et al.* (E93018), Separation of the longitudinal and transverse cross-sections in the $p(e, e'K^+)\Lambda$ and $p(e, e'K^+)\Sigma^0$ reactions, *Phys. Rev. C* **67**, 055205 (2003), [arXiv:nucl-ex/0211005](#).
- [202] G. Niculescu *et al.*, Longitudinal and transverse cross-sections in the $H-1(e, e' K+)\Lambda$ reaction, *Phys. Rev. Lett.* **81**, 1805 (1998).
- [203] C. J. Bebek, A. Browman, C. N. Brown, K. M. Hanson, R. V. Kline, D. Larson, F. M. Pipkin, S. W. Raither, A. Silverman, and L. K. Sistrong, Scalar-Transverse Separation of Electroproduced $K^+ \Lambda$ and $K^+ \Sigma^0$ Final States, *Phys. Rev. D* **15**, 3082 (1977).
- [204] D. Carman, private communication, (2023).
- [205] Jülich Supercomputing Centre, JURECA: Data Centric and Booster Modules implementing the Modular Supercomputing Architecture at Jülich Supercomputing Centre, *Journal of large-scale research facilities* **7**, [10.17815/jlsrf-7-182](#) (2021).

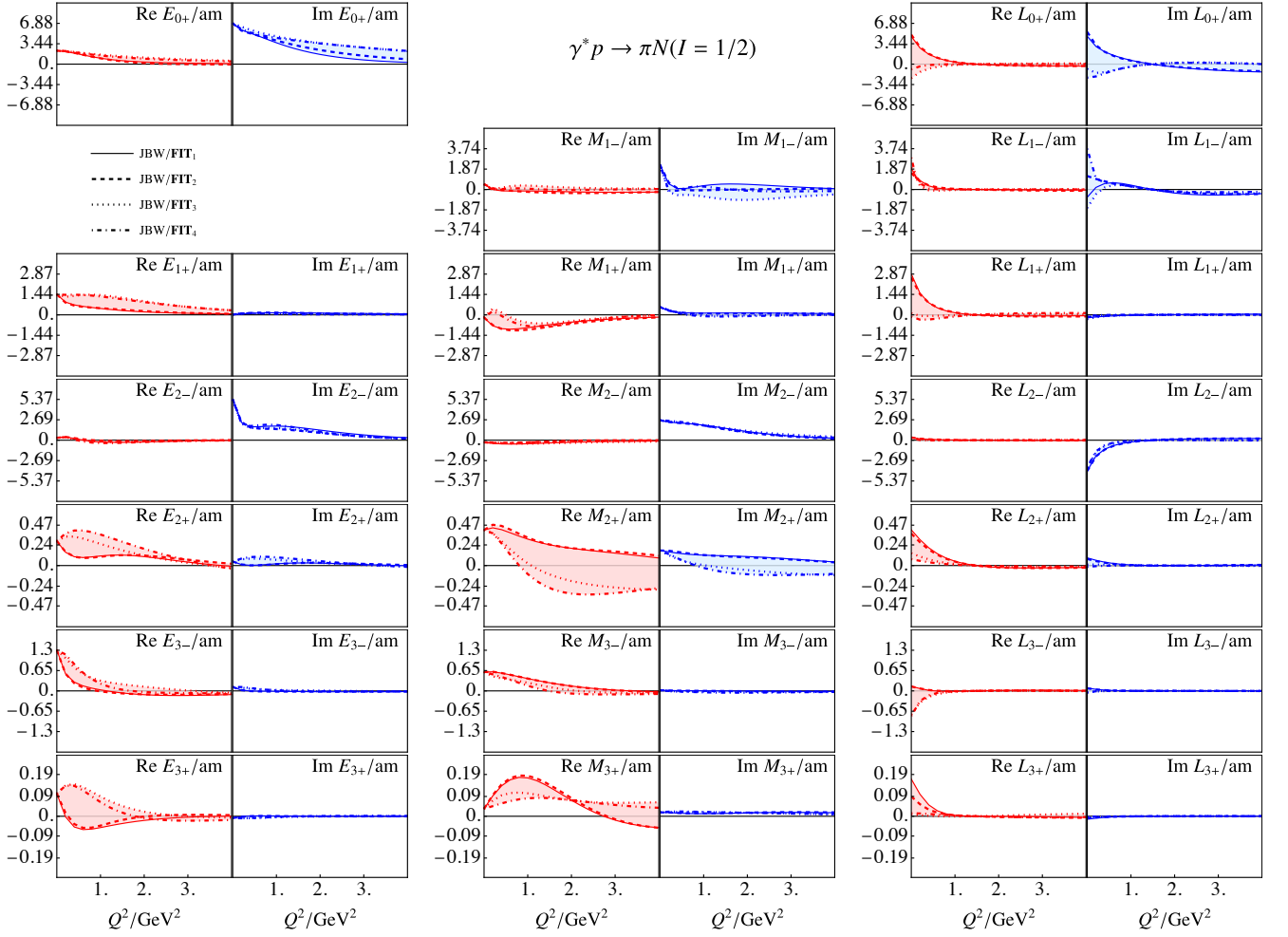
Appendix A: Multipoles at fixed W 

FIG. 12. Multipoles for the $\pi N(I = 1/2)$ final state obtained through JBW coupled-channel solutions (connected by the shading to guide the eye) including experimental data in $\pi N, \eta N, K\Lambda$ channels. Total energy is fixed to $W = 1.535$ GeV. Results at other kinematics can be obtained from the JBW web page <https://jbw.phys.gwu.edu>.

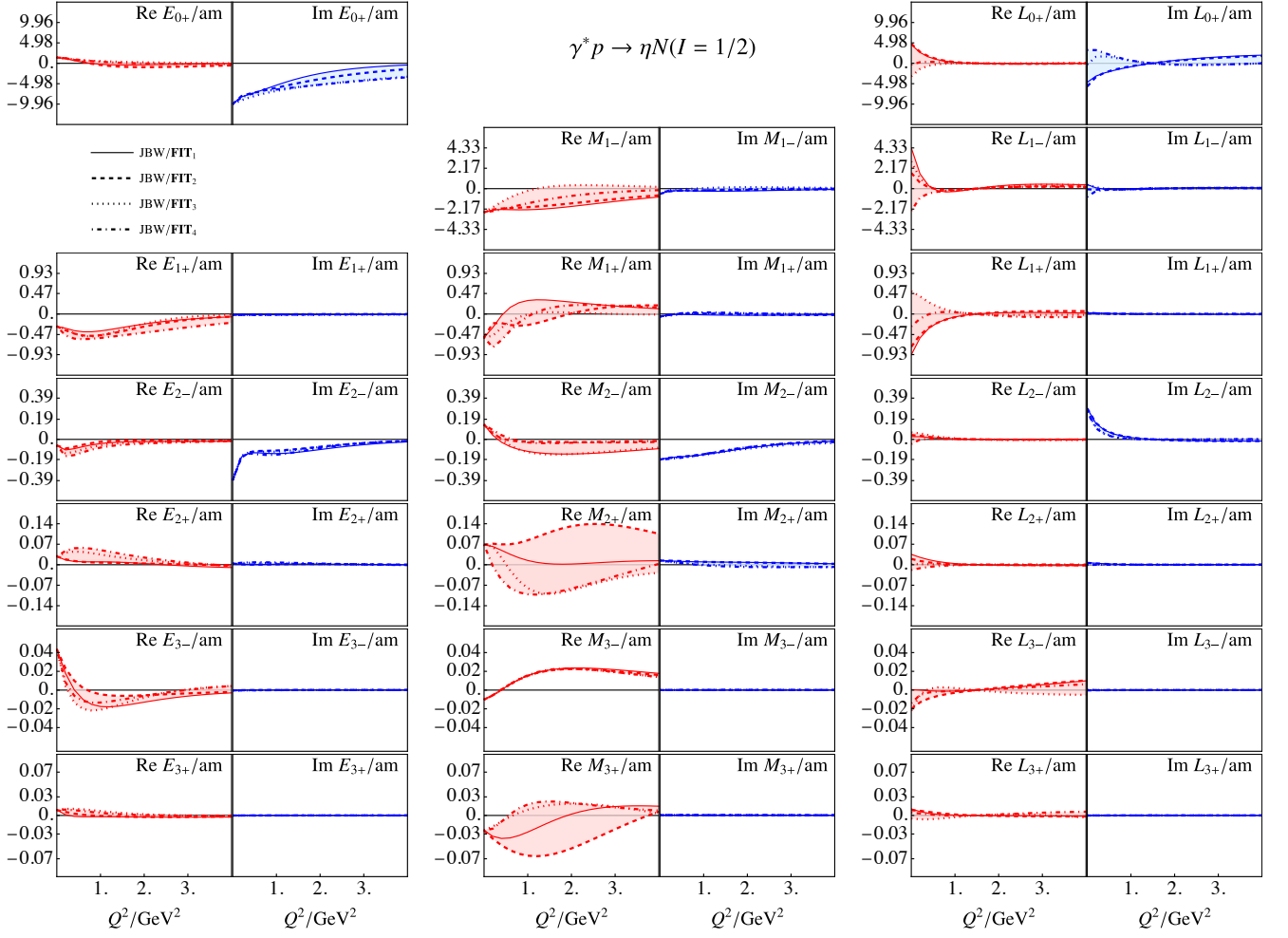


FIG. 13. Multipoles for the $\eta N(I = 1/2)$ final state obtained through JBW coupled-channel solutions (connected by the shading to guide the eye) including experimental data in $\pi N, \eta N, K\Lambda$ channels. Total energy is fixed to $W = 1.535$ GeV. Results at other kinematics can be obtained from the JBW web page <https://jbw.phys.gwu.edu>.